Microcrystallography Developments at the APS and Around the World

Robert Fischetti
X-ray Science Division and GM/CA
Advanced Photon Source

Outline

- Statistical highlights
- Aspects of micro-crystallography
- Scientific highlights
- Automation
- SONICC
- Micro-beams and radiation damage
- APS-U (150 mA)
- Putting it all in perspective

Macromolecular Crystallography at the APS

Operator	BM Line	ID Line(s)			Technique
BIOCARs	14-BMC	14-ID			MX, Laue, TR scattering, BSL2/3
IMCA-CAT	17-BM	17-ID			MX, 17-BM: powder diffraction
SBC-CAT	19-BM	19-ID			MX
LS-CAT		21-IDD	21-IDF	21-IDG	MX, Bionano-probe
SER-CAT	22-BM	22-ID			MX
GM/CA	23-BMB	23-IDB	23-IDD		MX, 23-BMB: WAXS
NE-CAT		24-IDC	24-IDE		MX
LRL-CAT		31-ID			MX

Beamlines previously used for MX

- 5ID
- 8BM
- 14-BMD

Beamtime request continue to grow

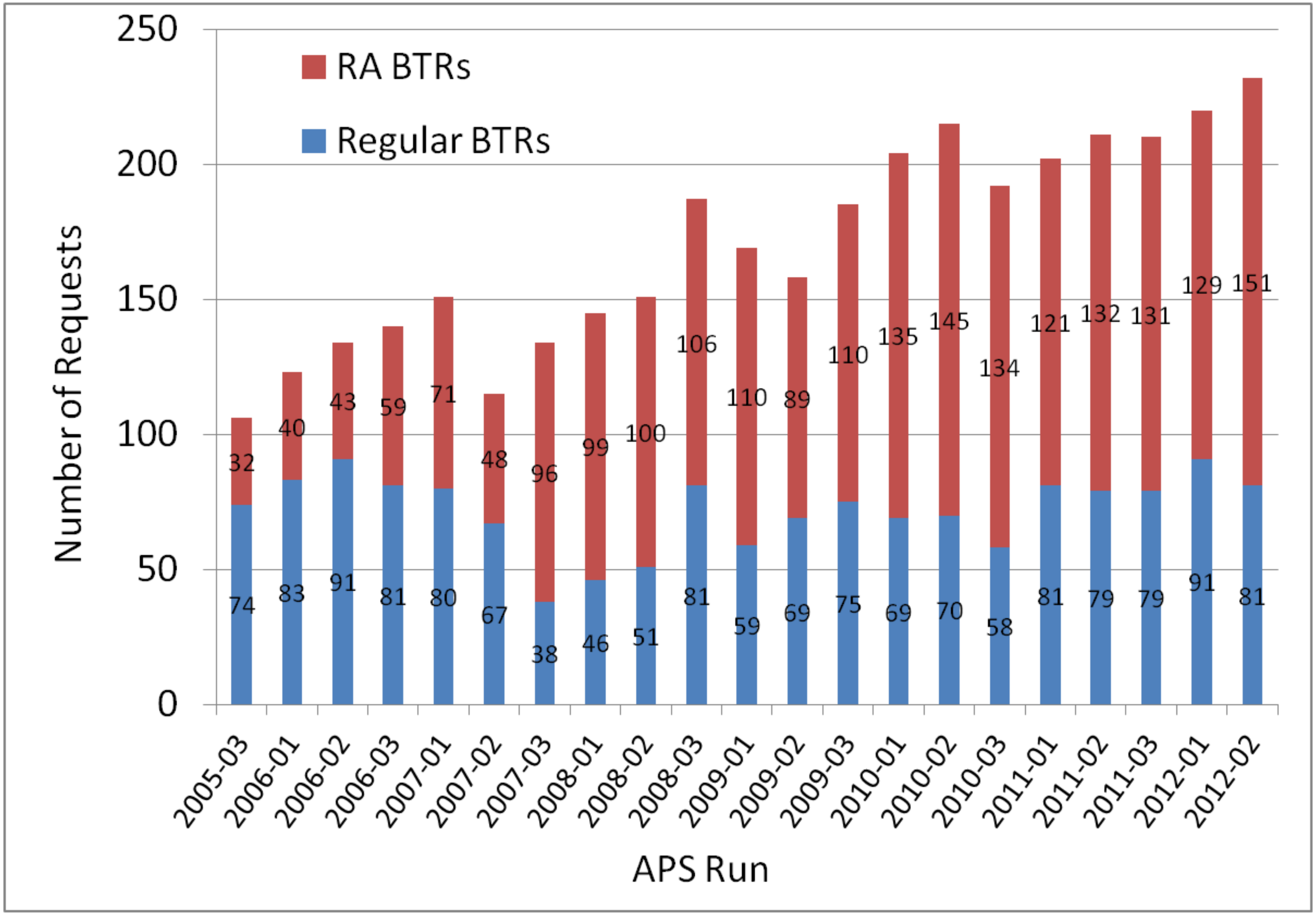

APS world leader in Protein Data Bank depositions

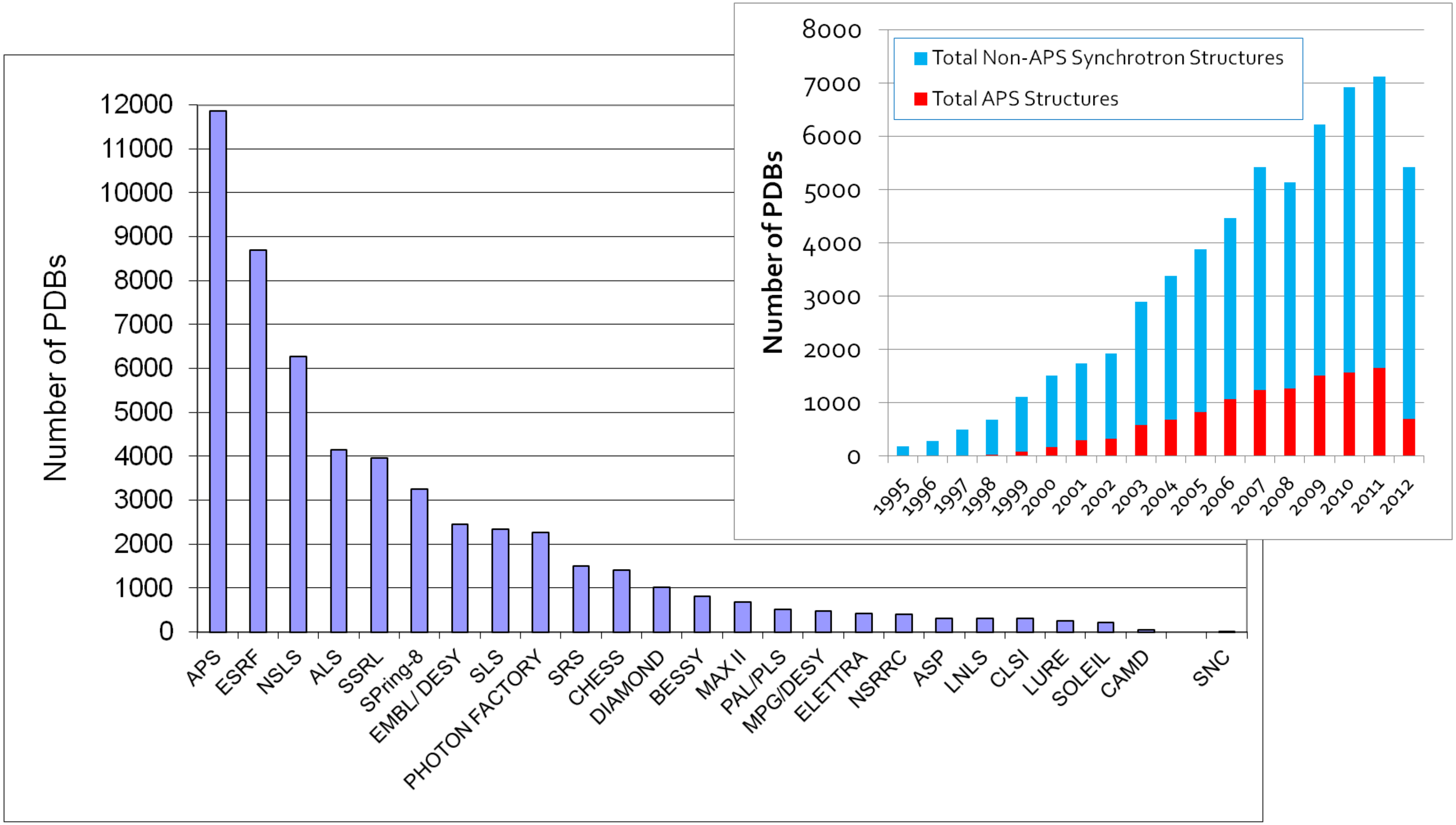

Over 25% of all structures from synchrotron source are from APS

1000 PDB club

APS 1000 PBD club membership

- SBC-CAT has 3629 deposits since 1997
- SER-CAT has 1943 deposits since 2002
- BioCARS has 1108 deposits since 1998
- IMCA-CAT has 1943 deposits since 1998
- GM/CA has 1005 deposits since 2005
- NE-CAT has 982 deposits since 2004
- LS-CAT has 905 deposits since 2008

National 1000 PDB club membership

- 5 [+ 2] sectors at the APS
- 2 sectors at ALS
- 3 sectors at NSLS
- 2 sectors at SSRL

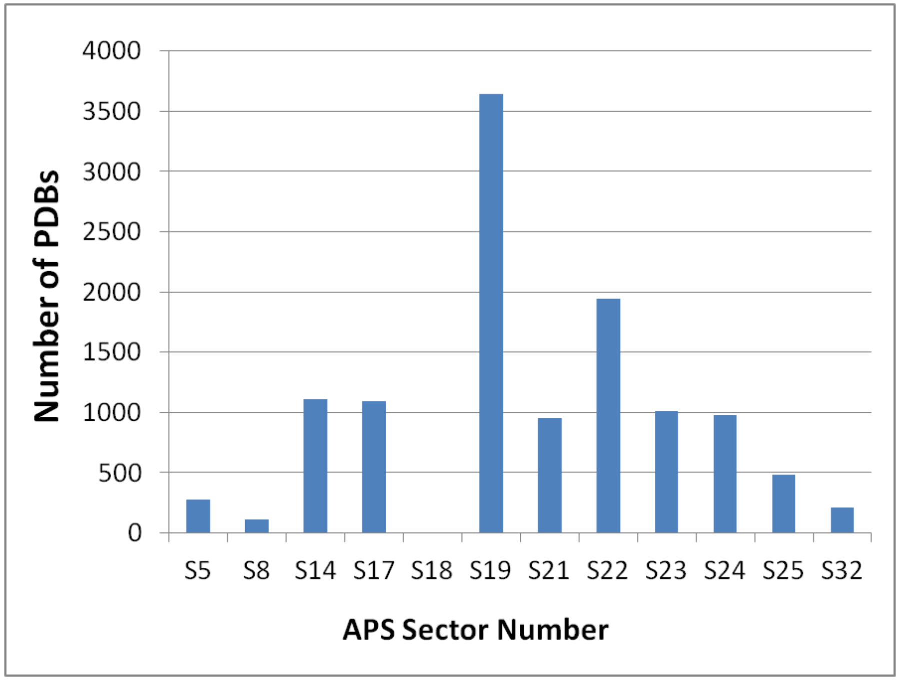

Micro-crystallography developments

On-axis sample visualization

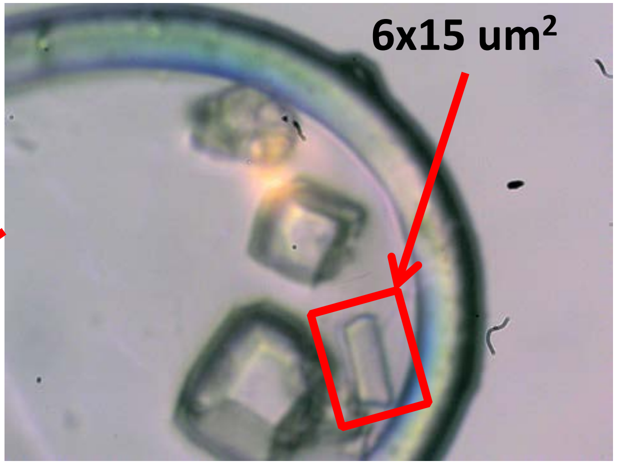

Goniometer:

1 µm SOC peak-to-peak

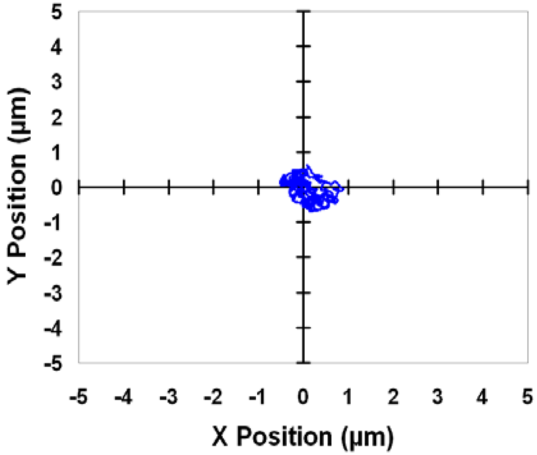

SONICC

Sample environment

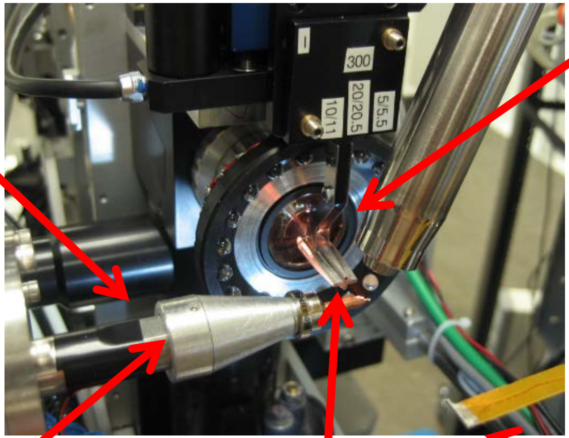

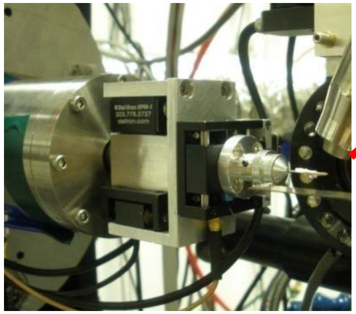

Goniometer head:
nano-positoning

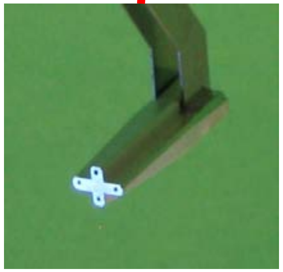

Quad mini-beam collimator:
5, 10, 20-µm beams and
300- µm scatter guard

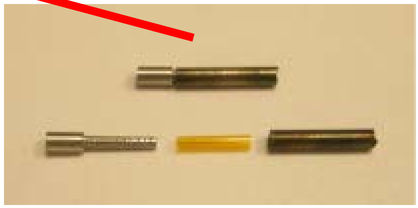

Active beamstop:
Photoelectric effect

Rapid beam size selection

JBluIce-EPICS GUI

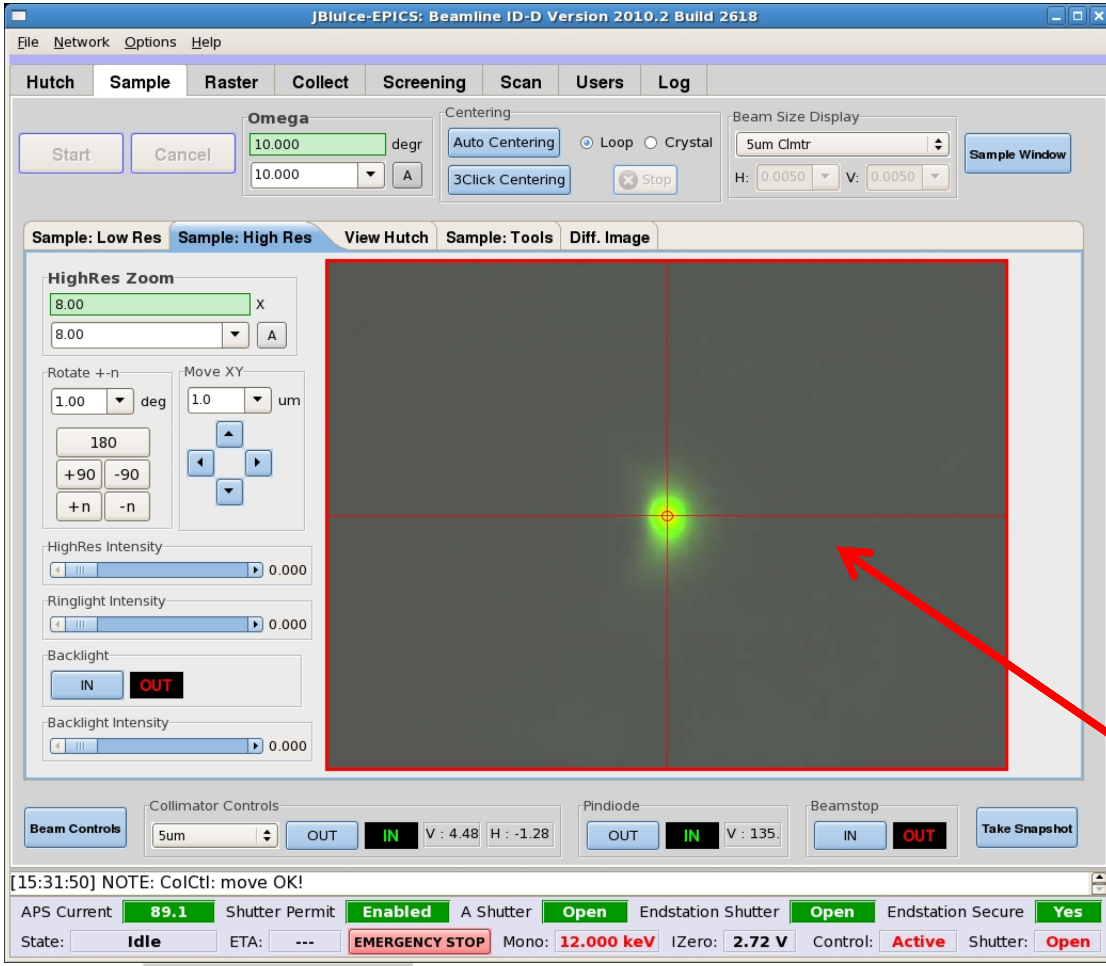

Beam size FWHM (μm)	Intensity (Ph./sec)
20 x 65	2.0 x 10^{13}
20 ∅	1.0 x 10^{12}
10 ∅	5.2 x 10^{11}
5 ∅	5.4 x 10^{10}
1 ∅	3.0 x 10^{9}

Image of beam at sample position on YAG crystal

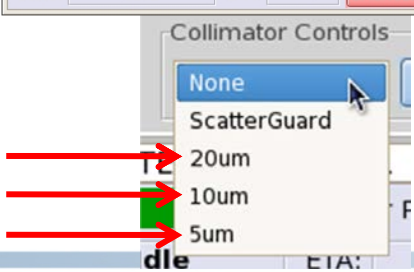

Quad mini-beam collimator
- match beam and crystal size
- use small beam to probe large crystal

Finding/centering invisible crystals or mapping quality

Grid search developed at ID13

Big beam – beam sample implemented at SSRL (*J. Syn. Rad*. (2007) **14**, 1891-195)

GM/CA large-beam (coarse grid) and mini-beam (fine grid) implementation (*J. R. Soc. (2009) Interface* , **6**, S587-S597)

Diamond and now many others have implemented rastering Acta Cryst. D, **66**, 1032-1035 (2010)

Ranking by "distl"
Nick Sauter

M.Hilgart, R.Sanishvili, C.Ogata, M.Becker, N.Venugopalan, S.Stepanov, O.Makarov, J.L.Smith, and R.F.Fischetti, Automated sample scanning methods for radiation damage mitigation and diffraction-based centering of macromolecular crystals, JSR (2011) 18, 717-722

Polygon rastering

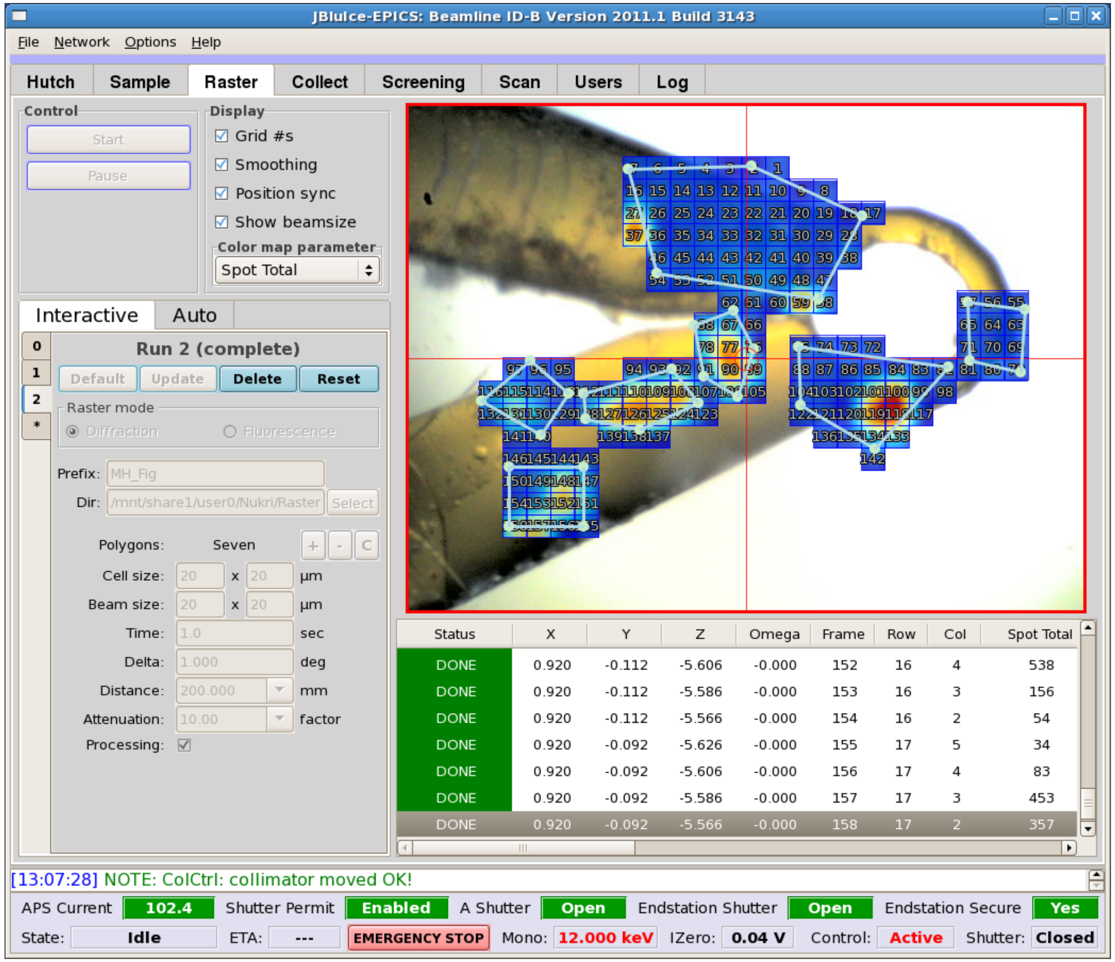

Coordinates can be transferred automatically for data collection

M.C. Hilgart, R. Sanishvili, C.M. Ogata, M. Becker, N. Venugopalan, S. Stepanov, O. Makarov, J.L. Smith and R.F. Fischetti J. Synchrotron Rad. (2011). 18, 717-722

Fluorescence rastering – fast slew scan mode

Slew mode ~30 sec

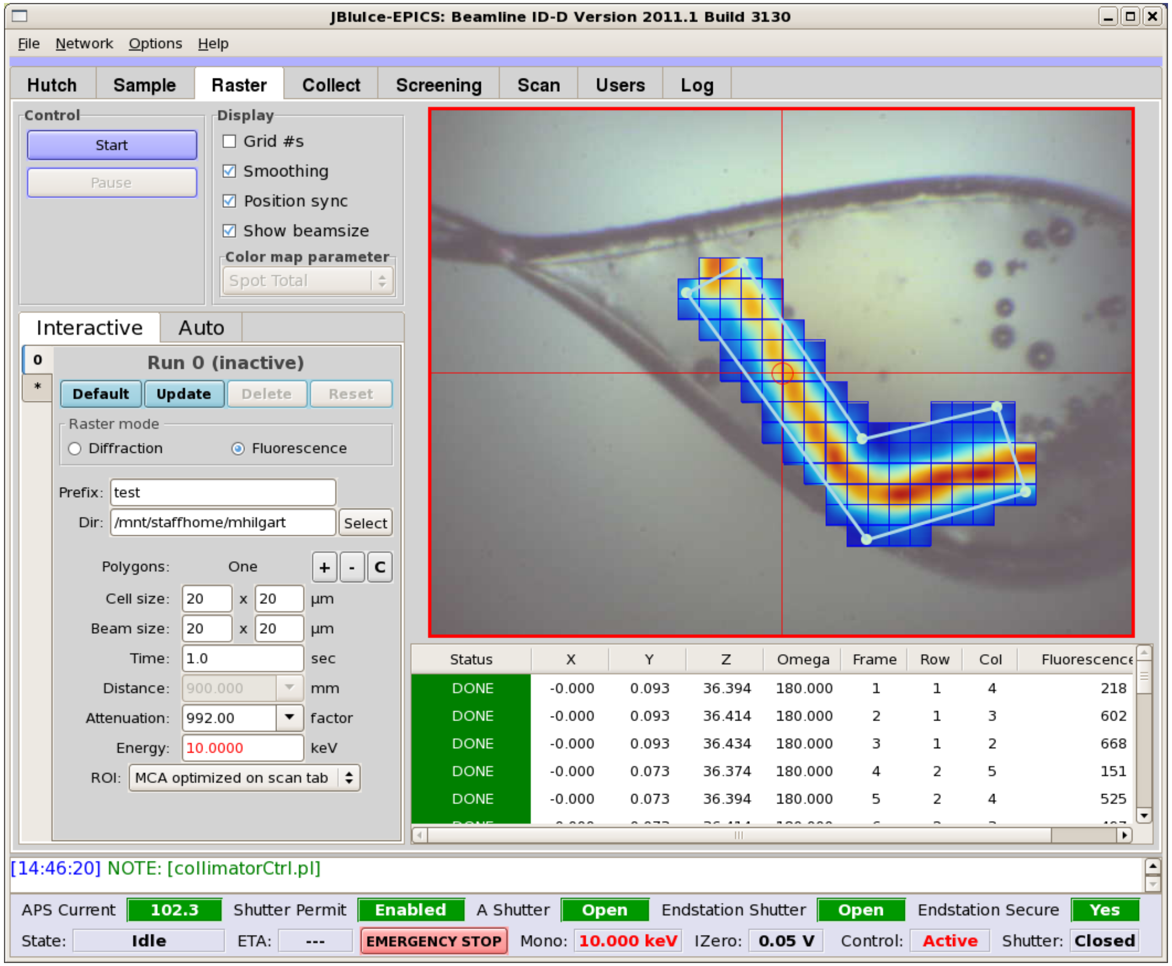

The cell and the beam size are 20µm.

Fast fluorescence techniques for crystallography beamlines Stepanov, S., Hilgart, M., Yoder, D., Makarov, O. Becker, M., Sanishvili, R., Ogata, C., Venugopalan, N., Aragão, D., Caffrey, M., Smith, J.L. and Fischetti, R.F. Acta. Cryst. D., **44**, 772-778, (2011).

AutoFind

- Produces a search area (polygon) definition
  - First performs optical centering if needed
  - Takes four images at angles 0, 30, 60, 90
  - Uses XREC to generate loop outline
  - Sets the sample to face-on orientation
  - Total time is about 40 seconds
- Adds a critical link from screening to analysis
- The next step in automation is to link this to the screening tab

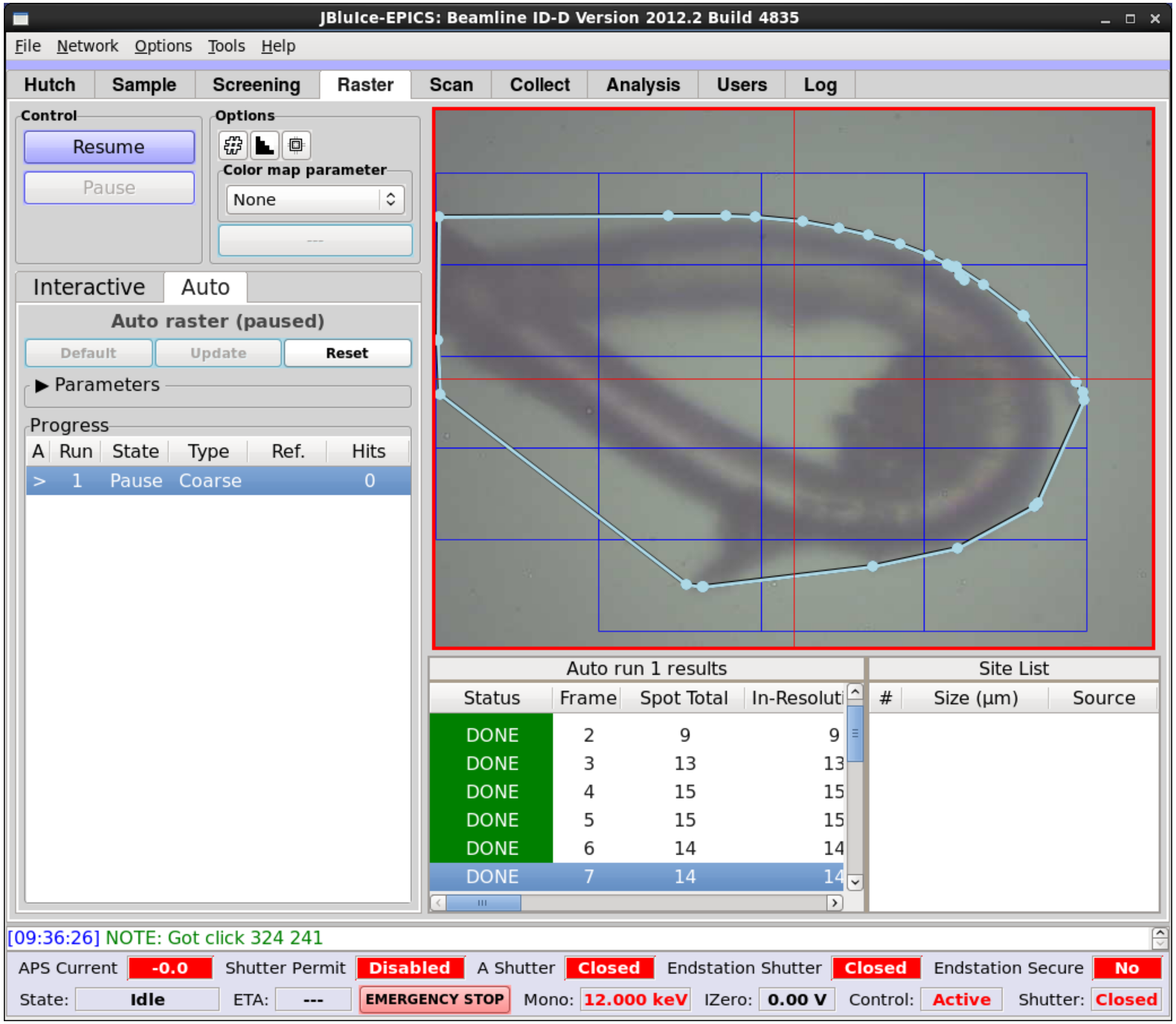

AutoFind automatically generates a search polygon

Dealing with radiation damage - automated collection along a user defined vector

Efficient use of large homogeneous crystals

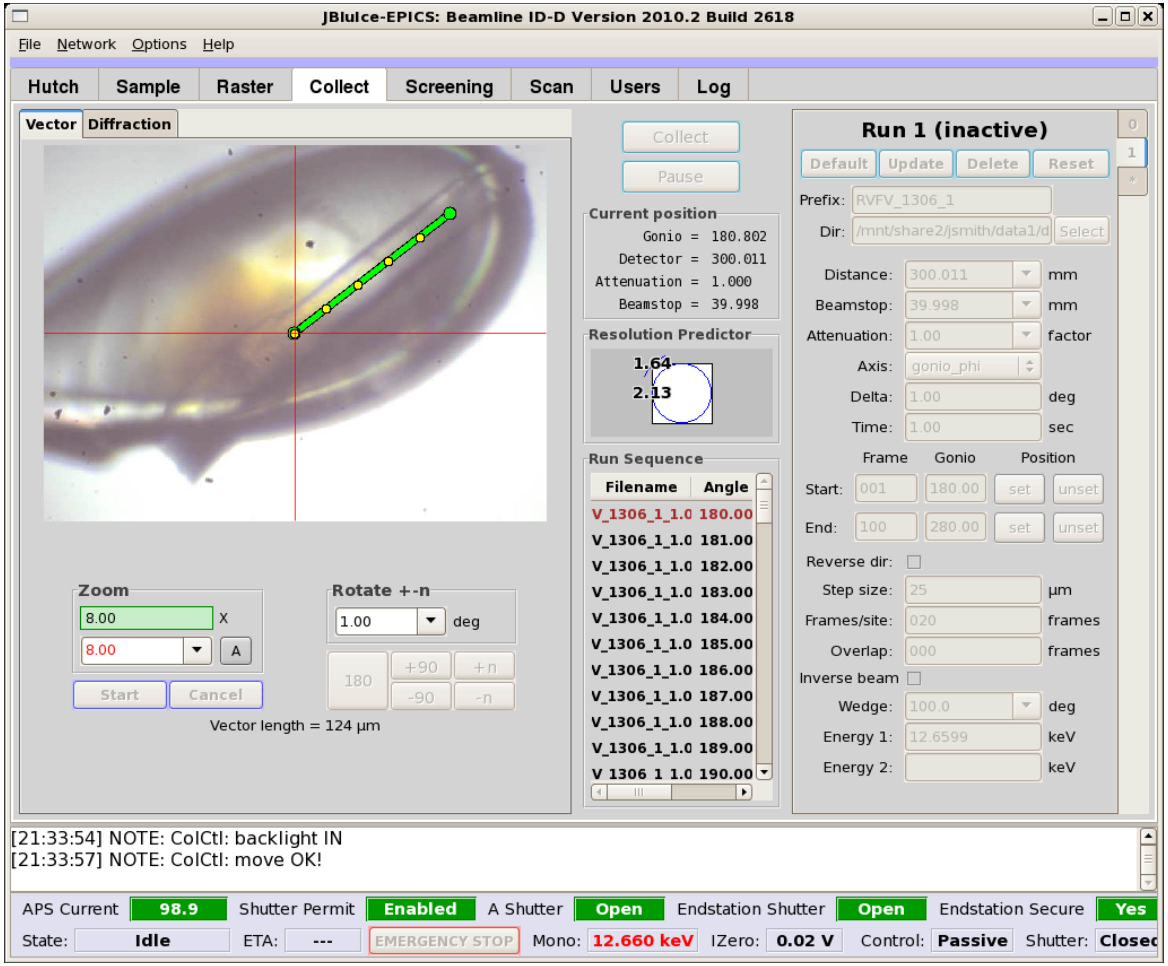

Mark Hilgart and Craig Ogata

Strategy Extended

- Multiple potential space groups are displayed with their associated strategy calculations
  - Solutions for each space group are computed in parallel
- Anomalous and inverse beam modes are supported
- MOSFLM or BEST can be chosen as the strategy program

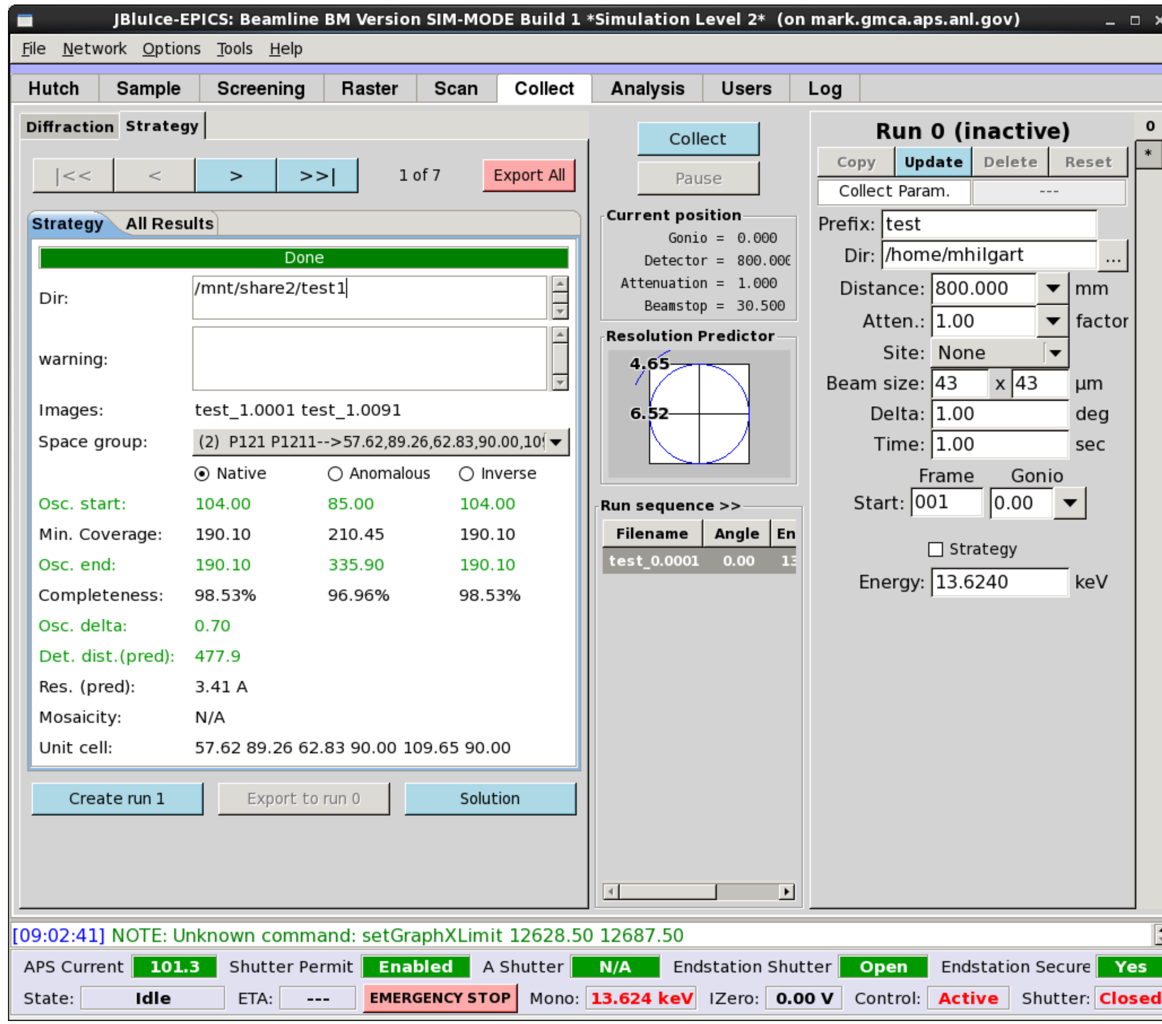

Analysis Tab

- XDS, POINTLESS, SCALA and TRUNCATE are run automatically in the background as each collect run completes
- Results populate the analysis tab as they finish
- Previous results can be flipped through using back/forward arrows
- An overview is shown along with graphs on the right
- Full text logs are available by clicking buttons at the bottom

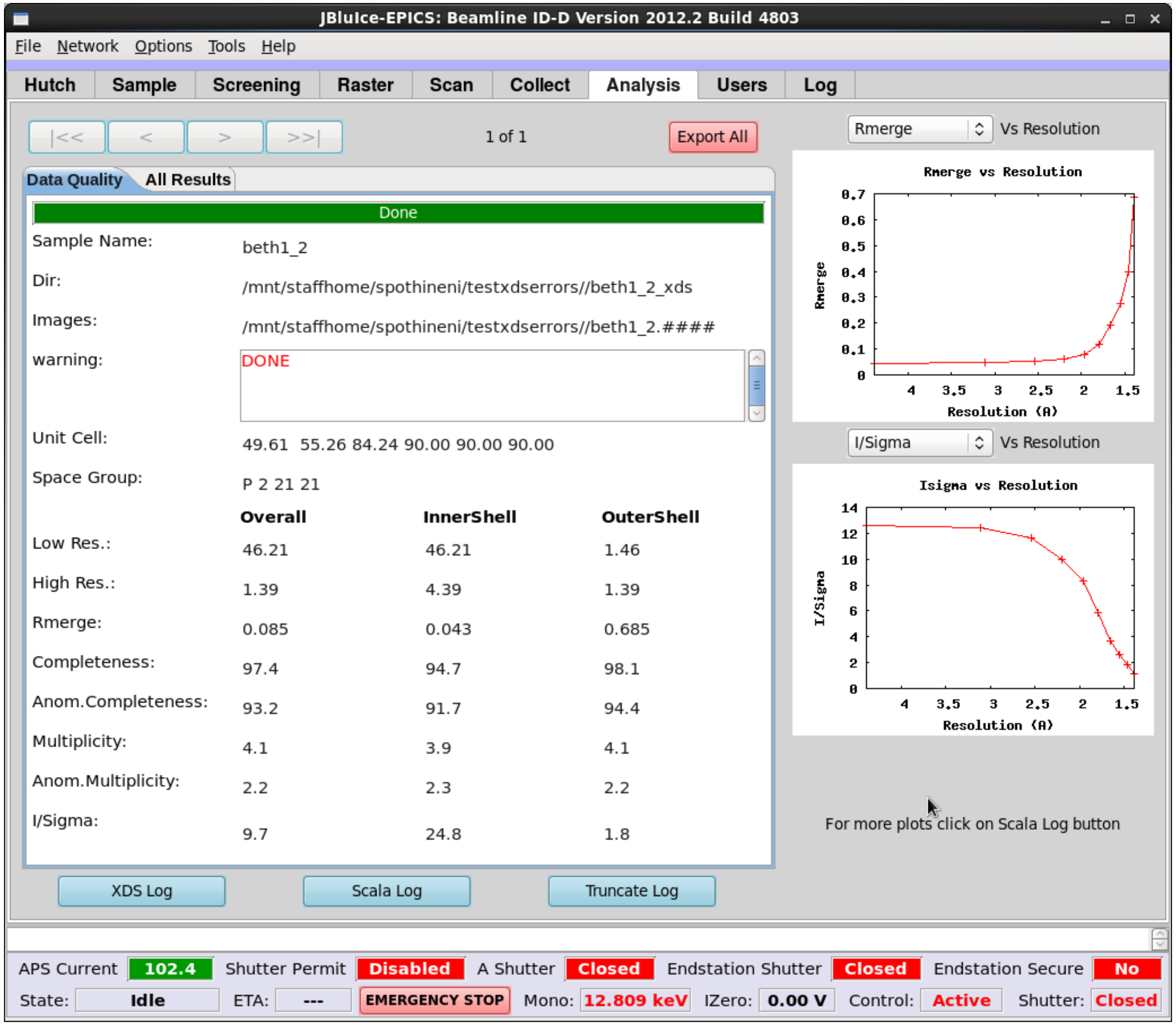

JBluIce-EPICS publications

Cherezov, V., Hanson, M.A., Griffith, M.T., Hilgart, M.C., Sanishvili, R., Nagarajan, V., Stepanov, S., Fischetti, R.F., Kuhn, P. and Stevens, R.C. (2009) Rastering strategy for screening and centering of microcrystal samples of human membrane proteins with a sub 10 micron size X-ray synchrotron beam,
J. R. Soc. Interface, 6 Suppl 5:S587-97 PMCID 2843980

Stepanov, S., Makarov, O., Hilgart, M., Pothineni, S., Urakhchin, A., Devarapalli, S., Yoder, D., Becker, M., Ogata, C., Sanishvili, R., Nagarajan, V., Smith, J.L. and Fischetti, R.F. (2011) JBluIce-EPICS control system for macromolecular crystallography,
Acta. Cryst. D67, 176–188 PMCID 3046456

Stepanov, S., Hilgart, M., Yoder, D., Makarov, O., Becker, M., Sanishvili, R., Ogata, C., Venugopalan, N., Aragão, D., Caffrey, M., Smith, J.L. and Fischetti, R.F. (2011) Fast fluorescence techniques for crystallography beamlines,
J. Appl. Cryst., 44, 772-778

Hilgart, M., Sanishvili, R., Ogata, C., Becker, M., Venugopalan, N., Stepanov, S., Makarov, O., Smith, J.L. and Fischetti, R.F. (2011) Automated sample scanning methods for radiation damage mitigation and diffraction-based centering of macromolecular crystals,
***J. Synchrotron Rad.* 18, 717-722** doi:10.1107/S0909049511029918

Video tutorials on-line and code is available for download

GM/CA co-sponsors with CCP4 a “hands on” school

www.gmca.aps.anl.gov

GPCR Highlights from 2012 GM/CA

A pair of u-opioid receptors

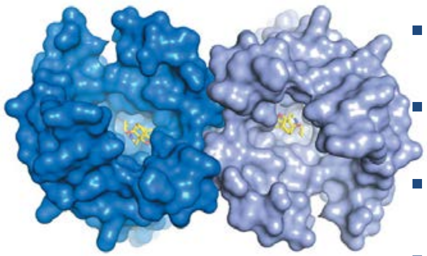

- Liu, W., …, Cherezov, V., and Stevens R.C. (2012), *Science* 337, 232-236.
  Human A_{2a} adenosine receptor
- Chun, E., …, Cherezov, V., Hanson, M.A., and Stevens, R.C. (2012), *Structure* 20, 967-976.
  Methods
- Manglik, A., …, Weis, W.I., Kobilka, B.K., and Granier, S. (2012), *Nature* 485, 321-326.
  μ-opioid receptor bound to a morphinan antagonist
- Wu, H., …, Cherezov, V., and Stevens, R.C. (2012), *Nature* 485**,** 327-332.
  Human κ-opioid receptor in complex with JDTic
- Thompson, A.A., …, Cherezov, V., and Stevens, R.C. (2012), *Nature* 485**,** 395-399.
  Nociceptin/orphanin FQ receptor in complex with a peptide mimetic
- Granier, S., ..., Weis, J. and Kobilka, B.K. (2012), *Nature* 485**,** 400-404.
  Delta-opioid receptor bound to naltrindole
- Kruse, A.C., …, Weis, W.I., Wess, J. and Kobilka, B.K., (2012), *Nature* 482**,** 552-556.
  M3 muscarinic acetylcholine receptor
- Haga, K., …, Weis, W.I., …, Kobilka, B.K., Haga, T., & Kobayashi, T., (2012), *Nature* 482**,** 547-551
  Human M2 muscarinic acetylcholine receptor bound to an antagonist
- Hanson, M.A., …, Kuhn, P., Rosen, H. and Stevens, R.C. (2012), *Science* 335, 851 – 855.
  Lipid G Protein-Coupled Receptor
- Li, D., Lee, J. and Caffrey, M. (2011), Cryst Growth Des 11, 530 – 537
  Methods
- Rasmussen, S.G., …, Weis, W.I., Sunahara, R., and Kobilka, B.K.(2011), *Nature* 477**,** 549-555
  β_2 adrenergic receptor-Gs protein complex

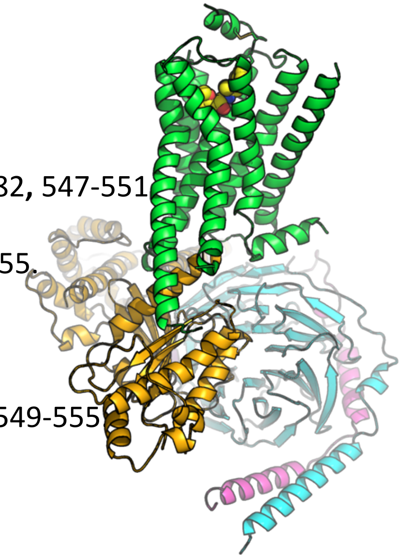

β_2 adrenergic receptor-Gs protein complex

Other Membrane Protein Publications

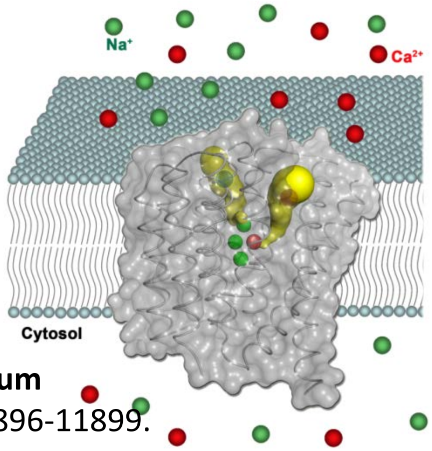

Crystal structure of the Na+/Ca2+ exchanger embedded in a membrane bilayer

- Liao, J., …, and Jiang, Y. (2012), *Science 335*, 686-690.
  Sodium/calcium exchanger
- Brohawn, S. G., …, and MacKinnon, R. (2012) , *Science 335*, 436-441.
  Human K2P TRAAK, a lipid- and mechano-sensitive K+ ion channel
- Whorton, M. R., and MacKinnon, R. (2011) , *Cell 147*, 199-208.
  Mammalian GIRK2 K+ channel and gating regulation by G proteins, PIP2, and sodium
- Uysal, S., …, Kossiakoff, A. A., and Perozo, E. (2011) , *Proc Natl Acad Sci U S A 108*, 11896-11899.
  Activation gating in the full-length KcsA K+ channel
- Shi, N., …, and Jiang, Y. (2011), *J Mol Biol 411*, 27-35.
  Determinants of K channel conductance and gating.
- Sauer, …, and Jiang, Y. (2011) , *Proc Natl Acad Sci U S A 108*, 16634-16639.
  Protein interactions central to stabilizing the K+ channel selectivity filter.
- Derebe, M. G., …, and Jiang, Y. (2011) , *Proc Natl Acad Sci U S A 108*, 598-602.
  Tuning ion selectivity of tetrameric cation channels by changing the number of ion binding sites
- Noinaj, N., ..., and Buchanan, S. K. (2012), *Nature 483, 53-58.*
  Structural basis for iron piracy by pathogenic Neisseria
- Fairman, J. W., ..., Cherezov, V., and Buchanan, S. K. (2012), *Structure 20, 1233-1243.*
  Outer Membrane Domain of Intimin and Invasin from Enterohemorrhagic E. coli and Enteropathogenic Y. pseudotuberculosis
- Oldham, M. L., and Chen, J. (2011), *P Natl Acad Sci USA 108*, 15152-15156.
  Maltose transporter during ATP hydrolysis
- Symersky, J., ..., and Mueller, D. M. (2012), *Nat Struct Mol Biol 19*, 485-491
  c(10) ring of the yeast mitochondrial ATP synthase in the open conformation
- Tiefenbrunn, T., ..., and Cherezov, V. (2011) , *PLoS One 6*, e22348.
  ba3 cytochrome c oxidase from Thermus thermophilus in a lipidic environment

Yeast mitochondrial ATP synthase c10-ring at pH 8.3

Thomas Schwartz (MIT): Structure of nucleoporin complex components

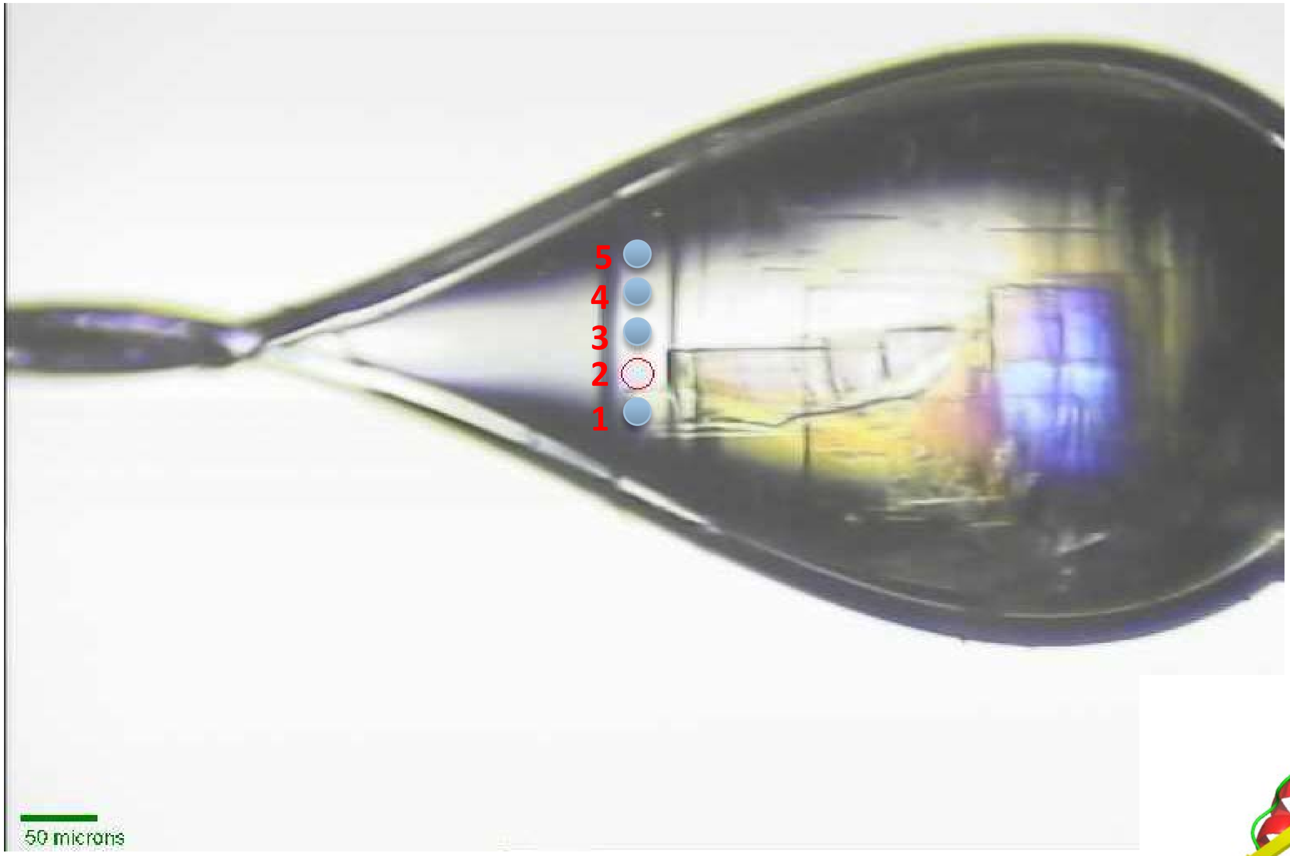

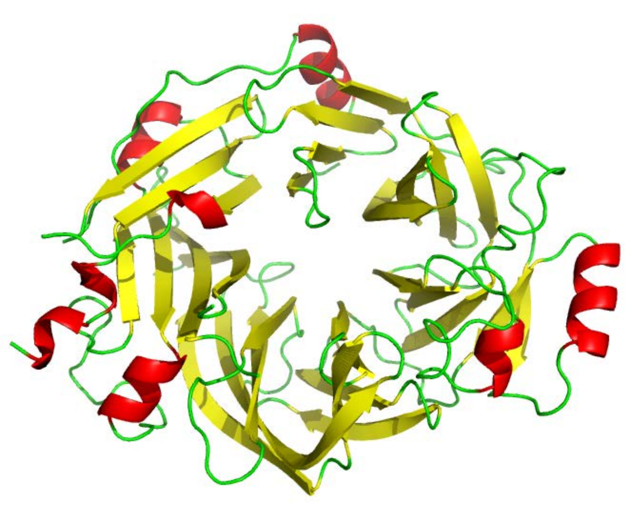

Space group $P2_1$, *a*=52, *b*=78, *c*=59Å, β=106º

NE-CAT

Automounter usage at GM/CA (% of user visits vs. APS trimester)

Over 90% of groups use the automounter
Over 40% collect data remotely
→ 5000 mounts/APS run cycle/beamline

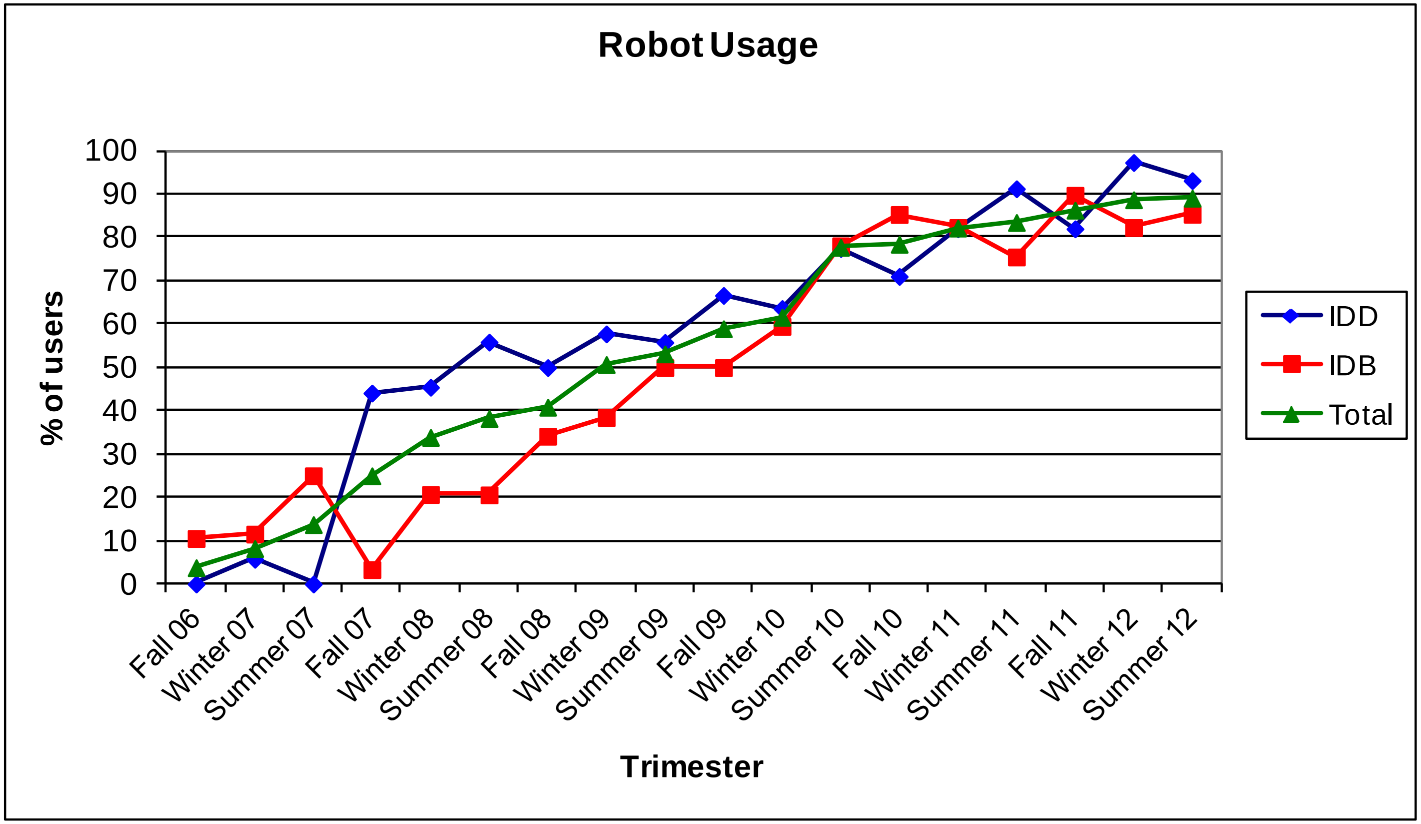

Craig Ogata

Berkeley Automounters

(T. Earnest and C. Cork)

Benefits:

- Larger Dewars
- Increased throughput
- Reduced vibrations
- Automated alignment

BAM-1 GM/CA modified Cartesian

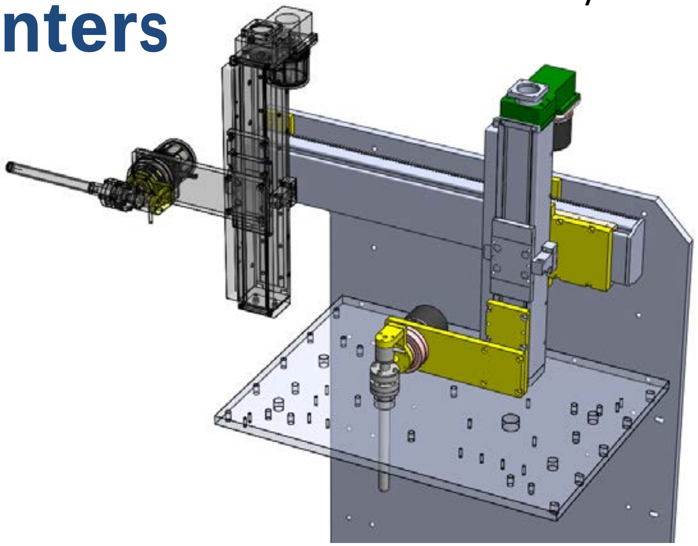

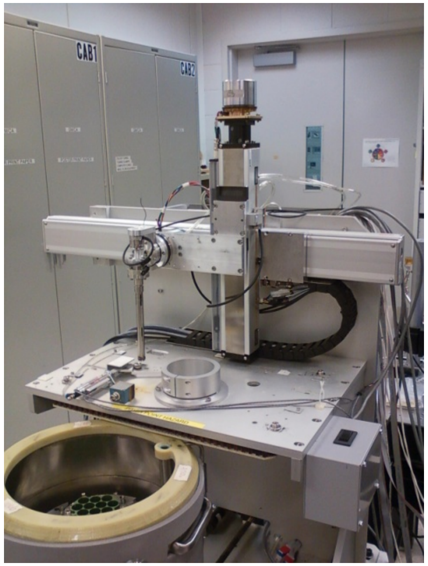

BAM-2 GM/CA Cartesian

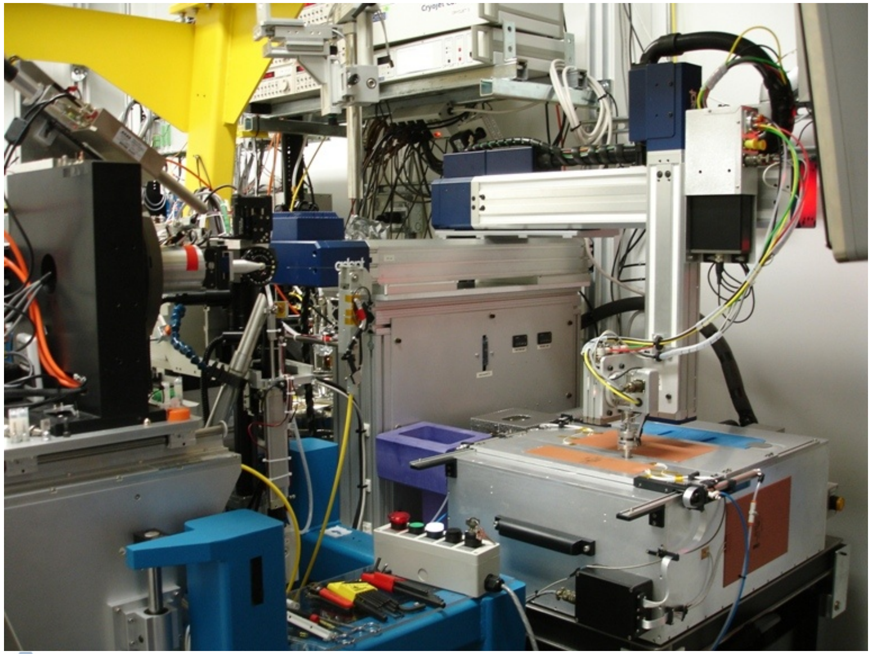

SER-CAT Cartesian w/ dual-Dewars

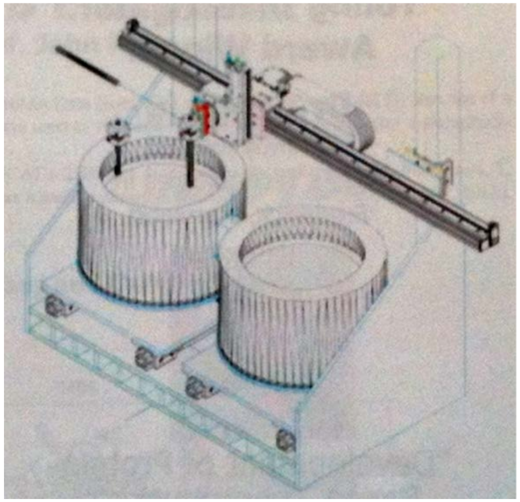

Do I have a crystal? Where is it?

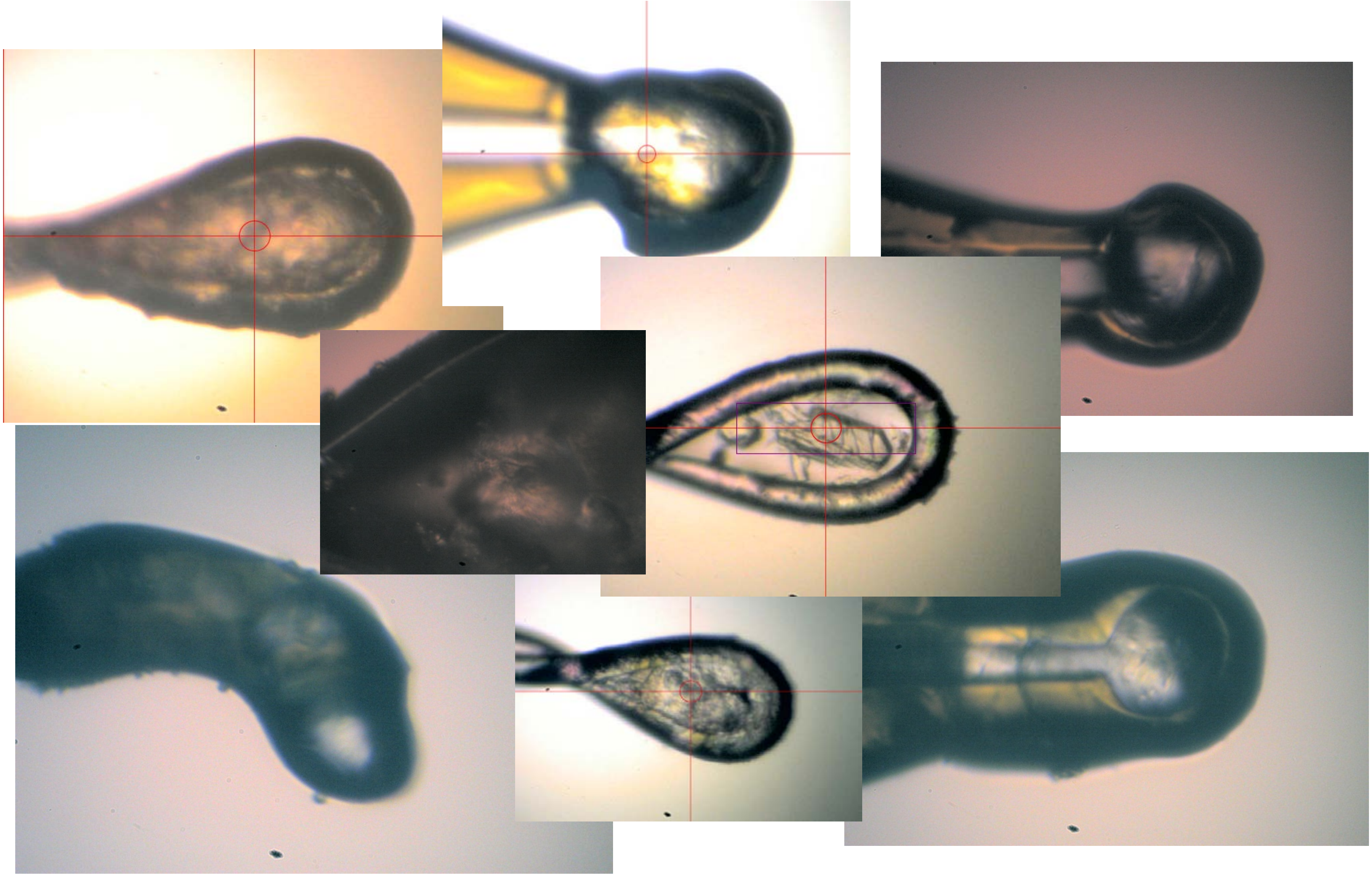

Chris Dettmar

SONICC on the beamline

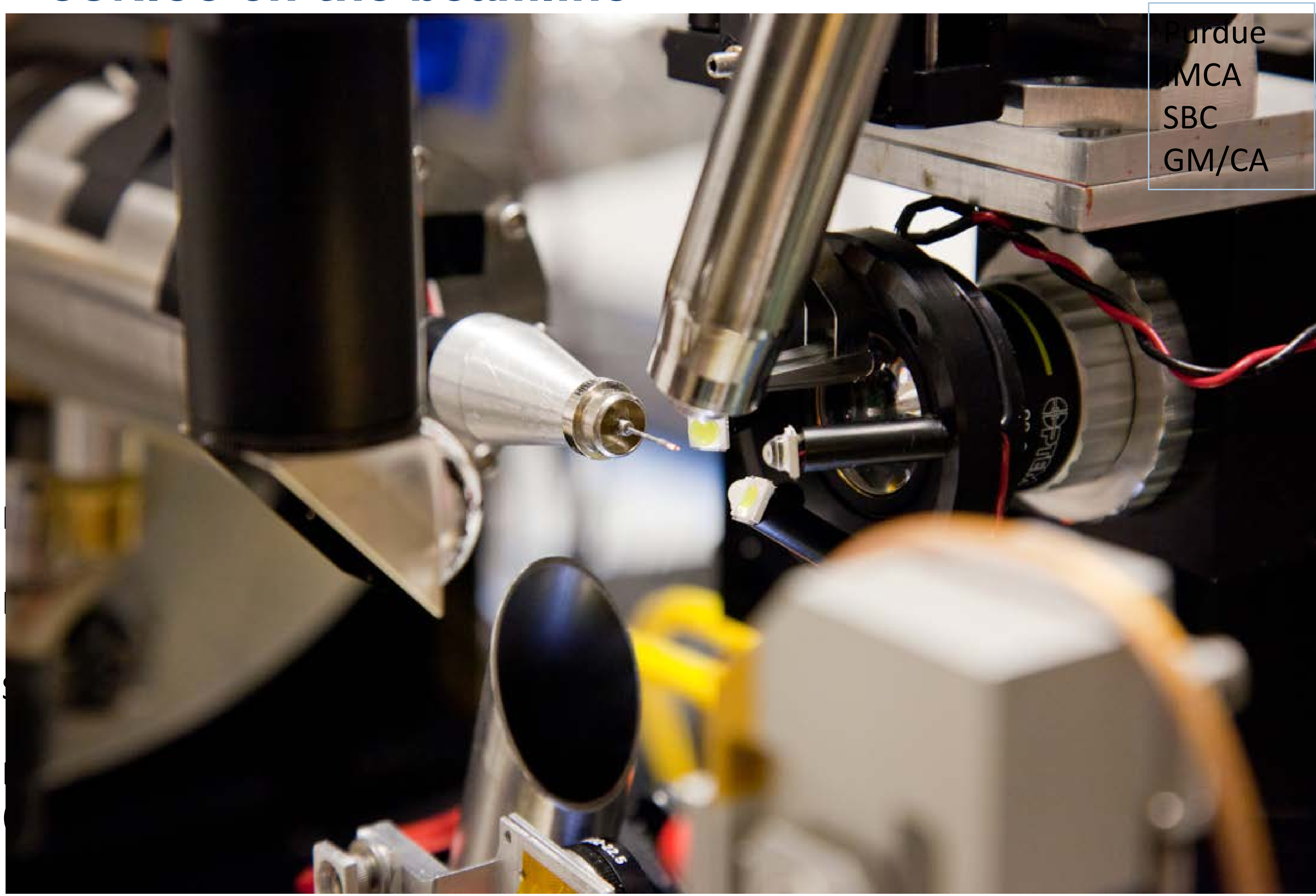

Purdue
IMCA
SBC
GM/CA

Mike Becker & Chris Dettmar

Faster, higher sensitivity detectors

CAT upgrades

BioCARS	Fast-CCD (on order)
IMCA	Pilatus 6M
SER-CAT	FAST-CCD (delivery soon)
GM/CA	Pilatus3 6M (on order)
NE-CAT	Pilatus-F 6M

Pilatus3 6M

- Improved dead time correction
- High count rate (10 MHz)
- High frame rate (100Hz)
- Improved efficiency with thicker sensor

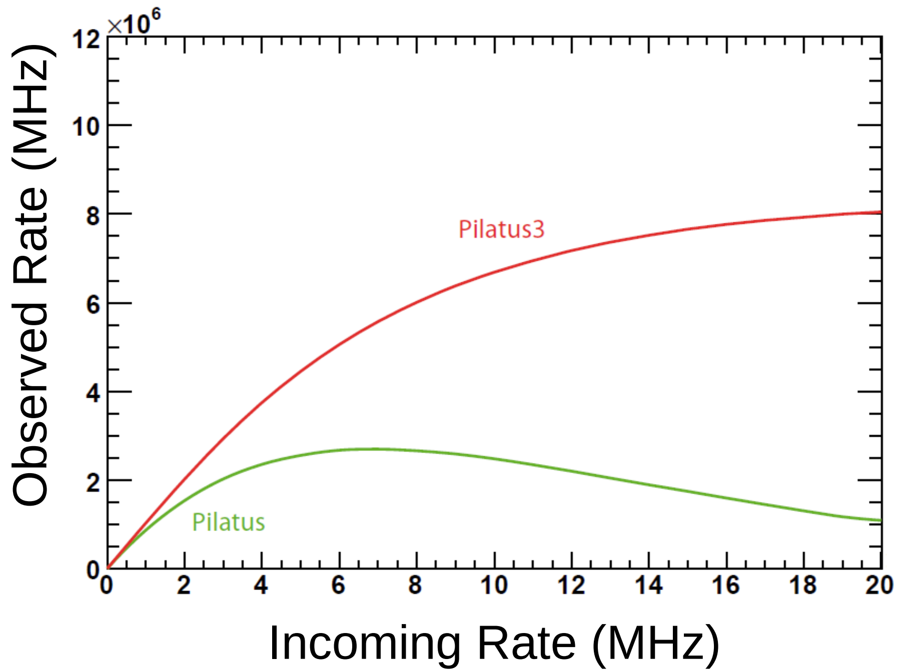

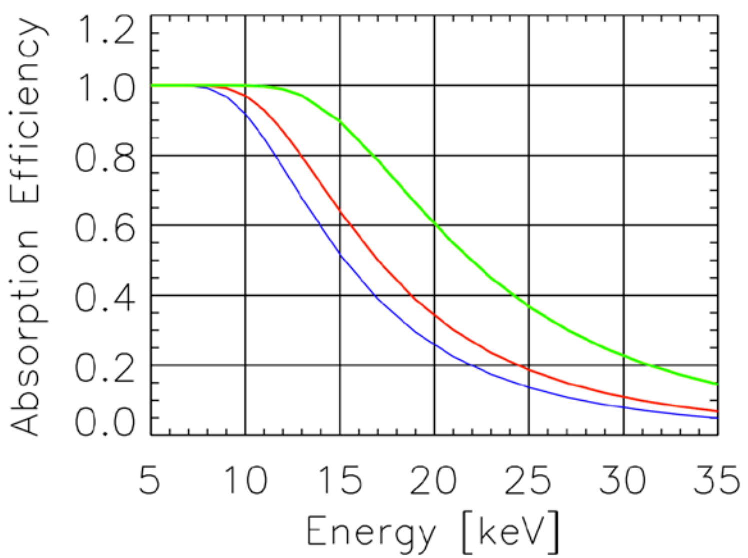

More efficient than 40 μm "thick" phosphor

Microfocus Upgrade Motivation

Provide more intensity for challenging projects
- Membrane proteins in meso-phase
  - Small (5-10 µm) and weakly scattering crystals

Provide routine access to microfocus beam - ~1 µm

Exploit APS high energy source properties
- Provide high energy and/or small beams
- Study radiation damage at higher energies

Radiation damage

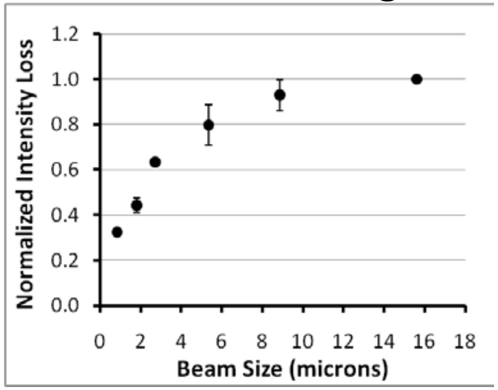

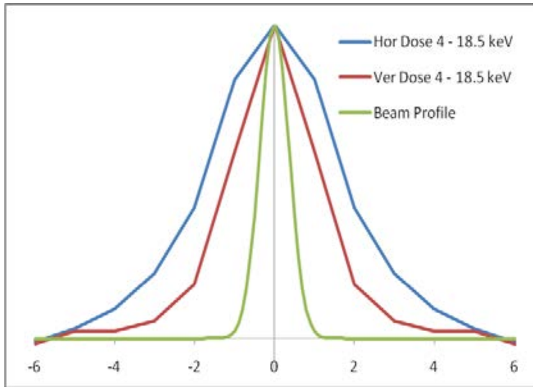

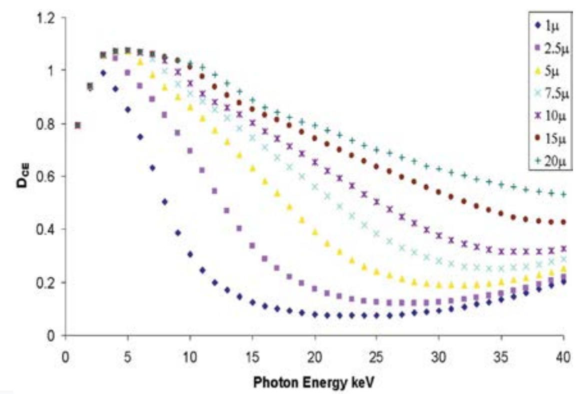

µ-opioid GPCR
Brian Kobilka's lab

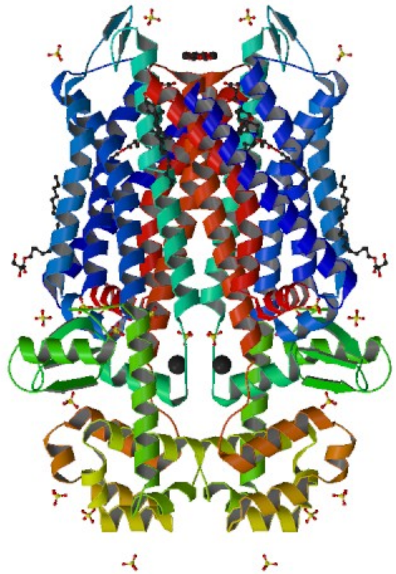

k-opioid GPCR
Ray Steven's lab

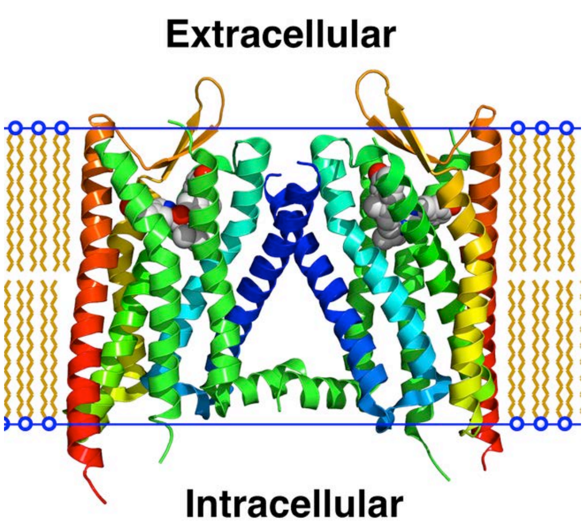

Microfocus Upgrade Optical Specifications

Optical Specifications

Beam size (FWHM):

micro-beam mode - beam size can be varied from 1 – 5 µm in a few seconds

mini-beam mode - beam size can be varied from 3 – 20 µm in a few seconds

mode switch <10 minutes

Energy range: 6 – 35 keV

using Si(111) and Si(333)

or Si(311)

Harmonic rejection

$>10^2$

existing KBM system will provide sufficient harmonic rejection

Intensity in 1 µm beam at sample position:

2×10^{10} photons/s, < 500 μrad^2 @ 12.0 and 18.5 keV

5×10^{10} photons/s, < 1000 μrad^2 @ 12.0 and 18.5 keV

Increase mini-beam intensity 5-fold over current 23-ID-D

Positional stability: 10% RMS of focal size, 1 – 100 Hz

Intensity stability: 1% RMS noise, 1 – 100 Hz

Microfocus Upgrade Layout

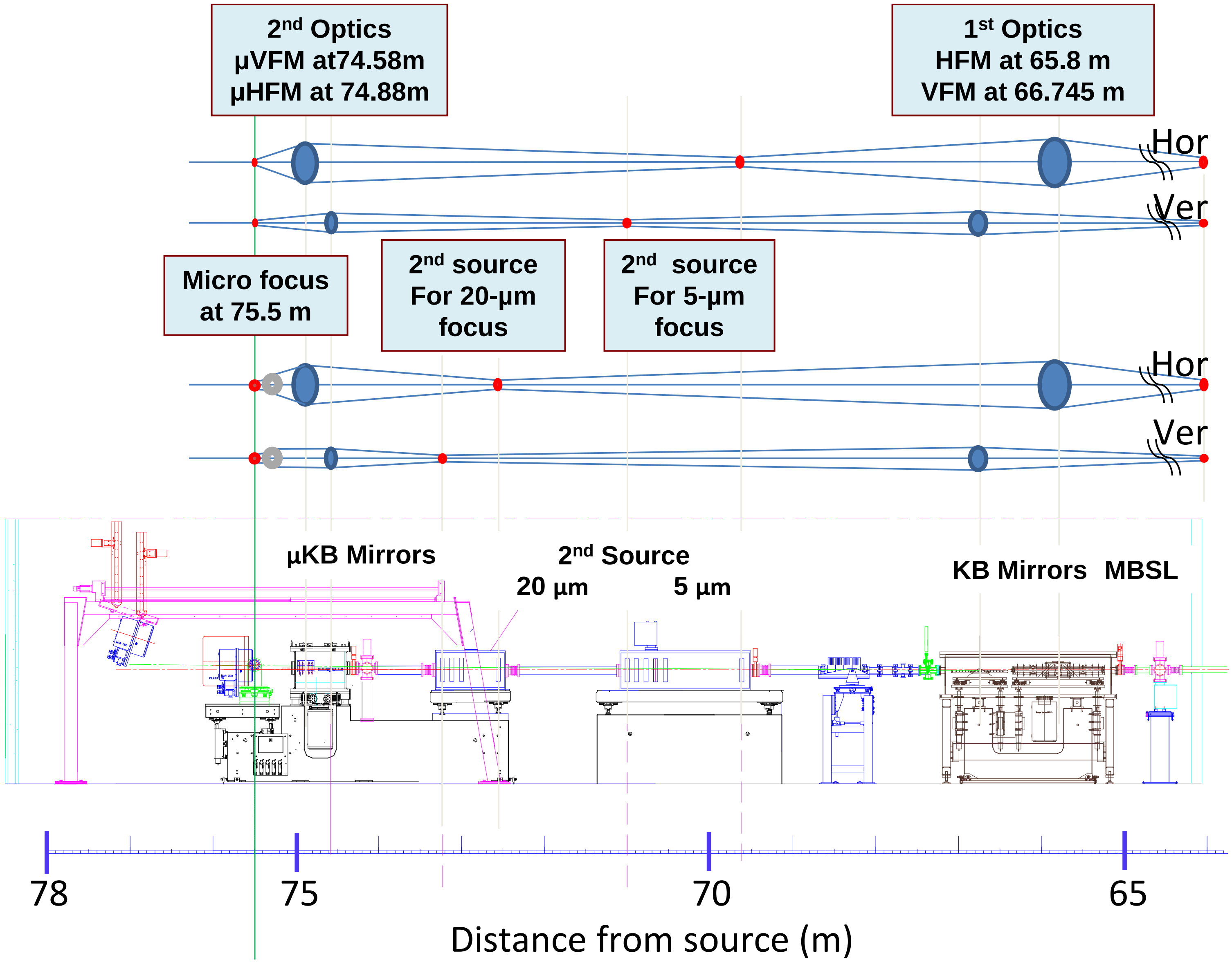

Microfocus Upgrade: Intensity vs. Energy

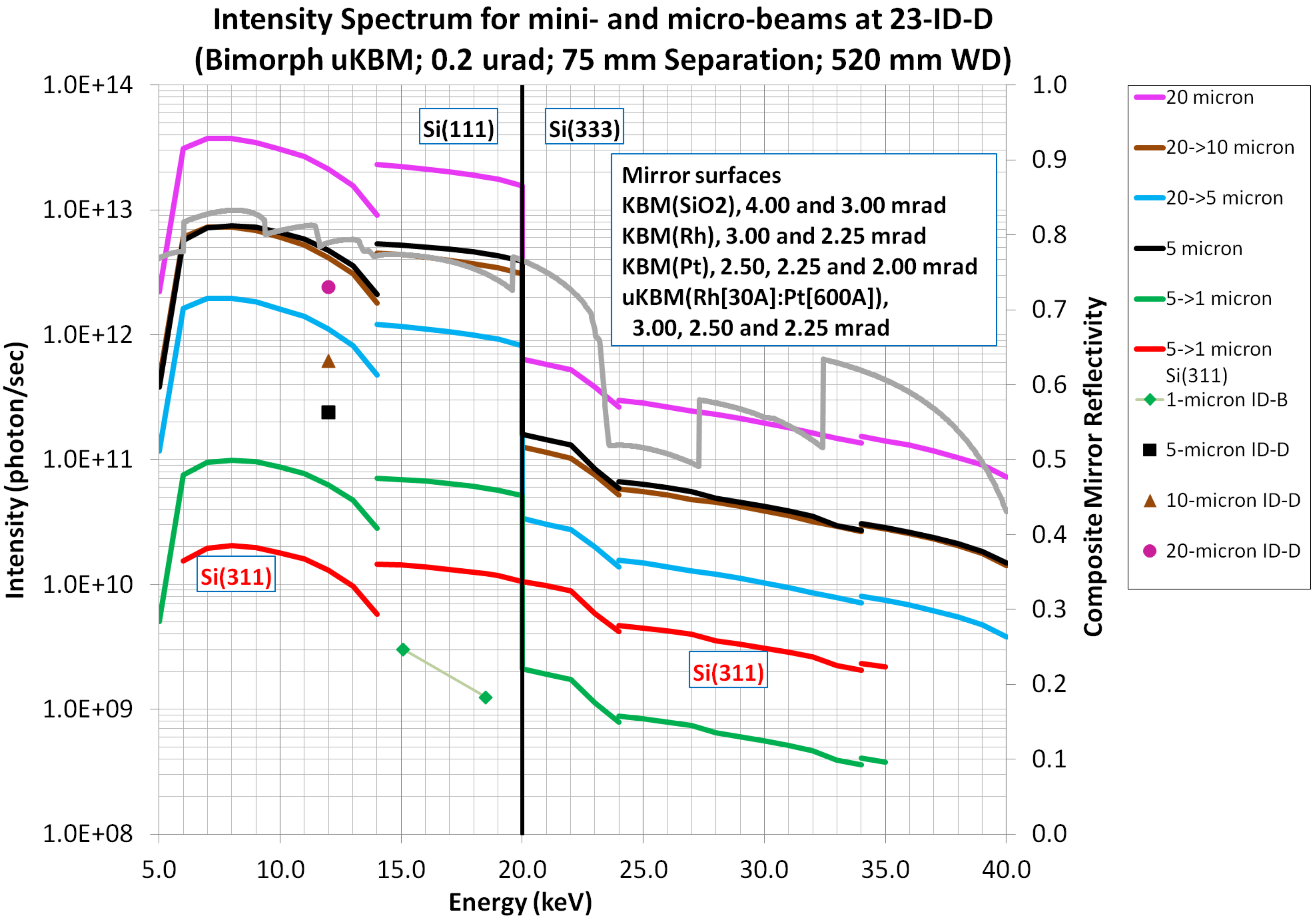

Air bearing performance

NELSON AIR CORP.
precision air bearing positioning

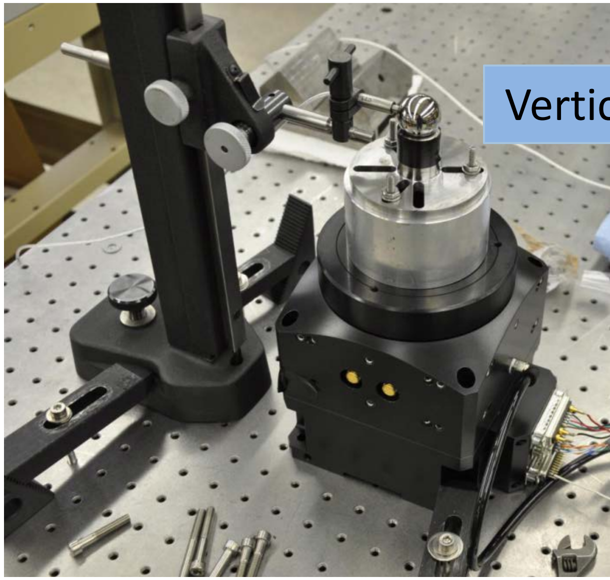

Vertical axis

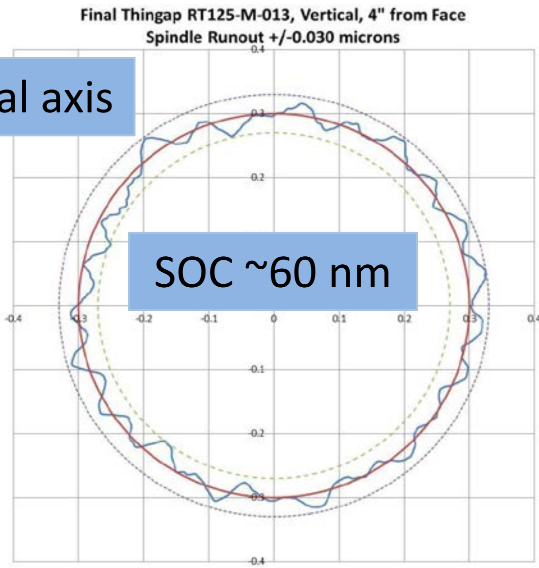

SOC ~60 nm

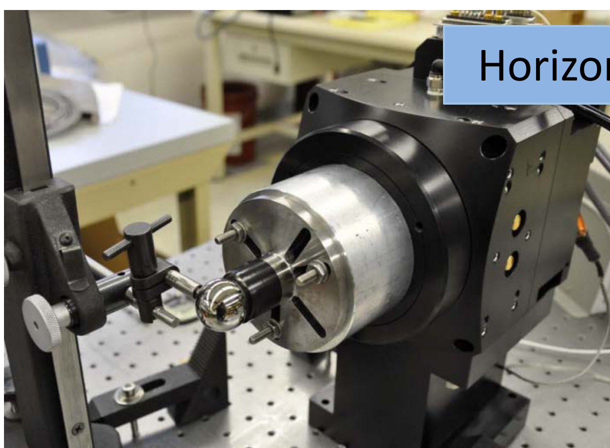

Horizontal axis

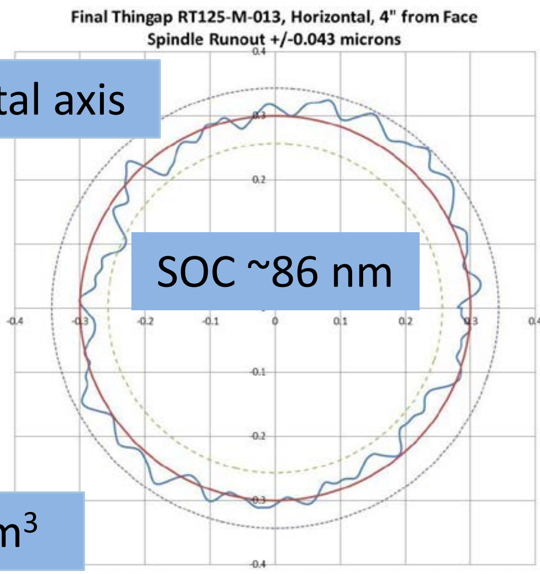

SOC ~86 nm

Dimensions: 140 x 140 x 165 mm^3

SOC ~100 nm

SOC measurements
- 100 mm off face
- peak-to-peak
- mostly synchronous error

Intensity loss as a function of beam size and dose

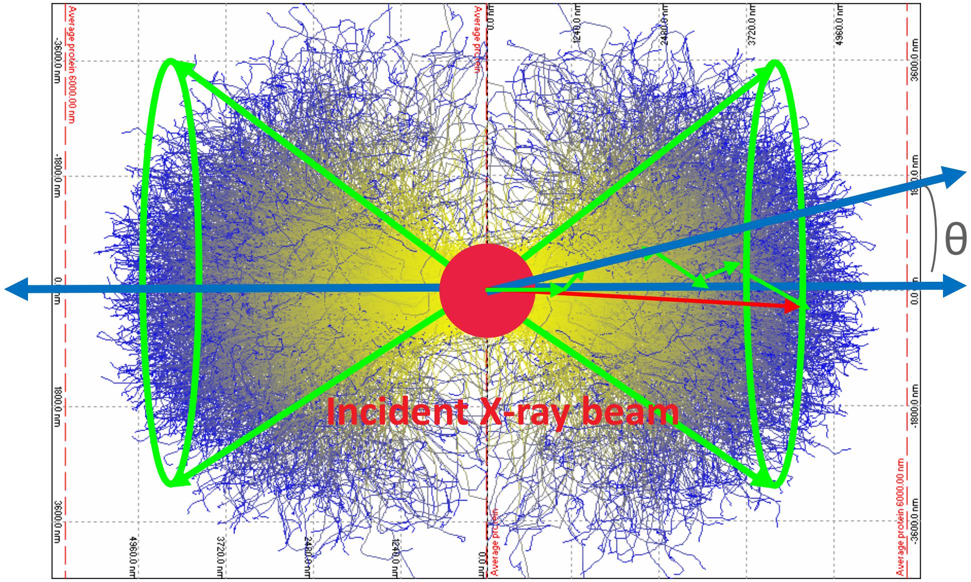

Damage decreases 3-fold with beam size

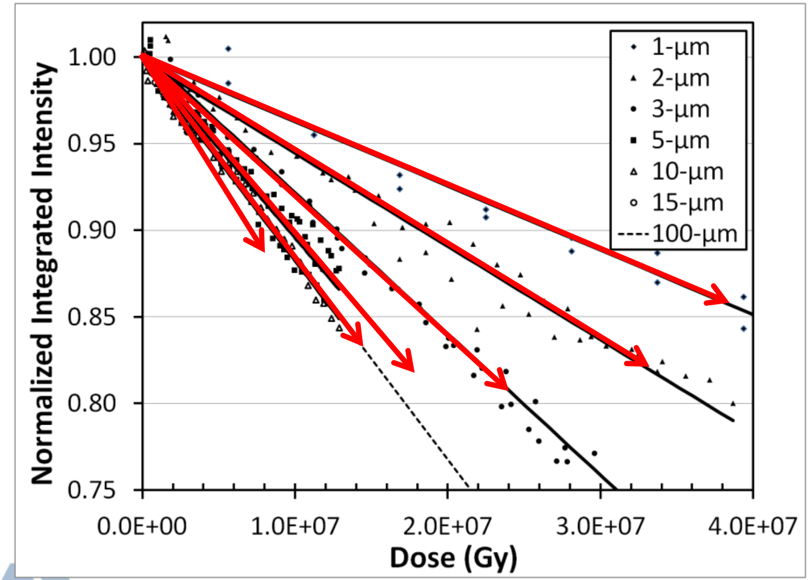

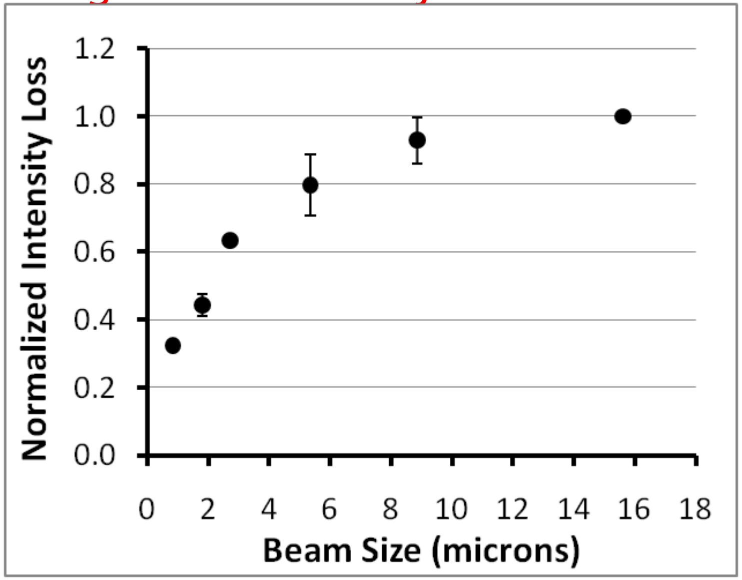

Nukri Sanishvili and Derek Yoder

Distribution of damage is wider than beam

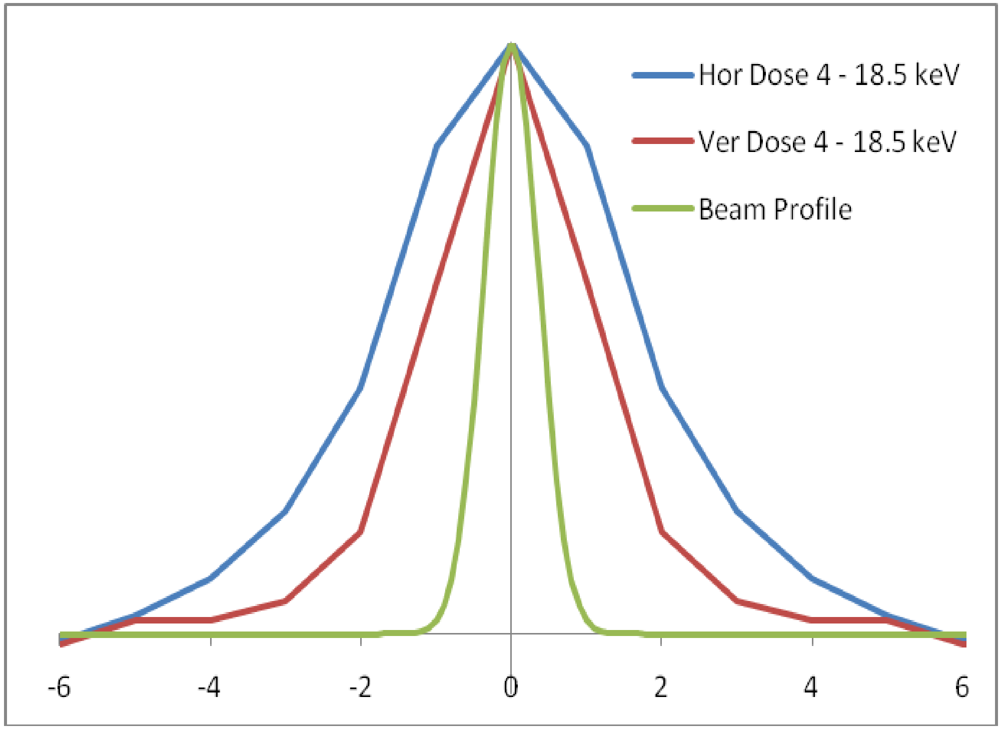

Photoelectron
CSDA ~8 µm
Monte Carlo ~4 µm
Auger ~0.1 µm
Compton

	HWHM (µm)	Ratio
Beam profile	0.42	1.0
Horizontal distribution	2.02	4.8
Vertical distribution	1.19	2.8

Mitigation of Radiation Damage Using Line Focus Beam

- A new strategy to reduce primary X-ray damage in macromolecular crystallography uses the basic principle of separating, as much as possible, the X-ray irradiated region, where the diffracted signal originates, from the region where damage accumulates.
- Photoelectrons causing radiation damage accumulate predominantly outside the irradiated region of the crystal exposed with a line focused beam leading to a 4.5 factor decrease in radiation damage.

Experiment

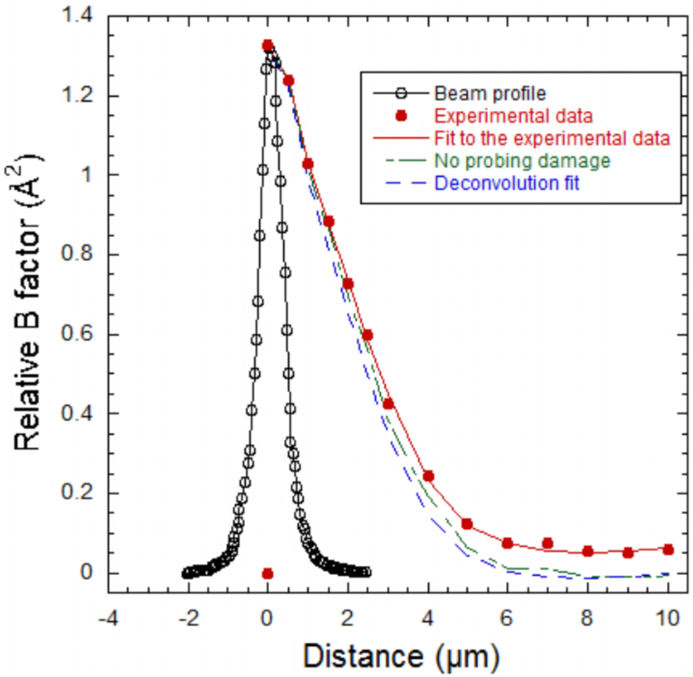

Plots of the measured lens focus profile, spatial dependent damage, the deconvoluted spatial dependent damage, and the spatial dependent data with the probing damage removed.

Simulation

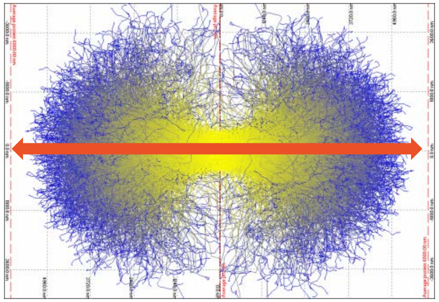

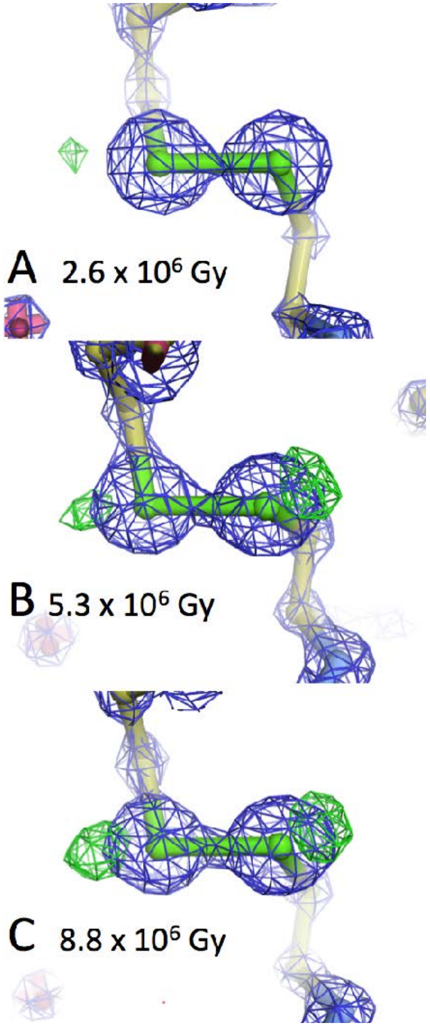

Electron density maps contoured at 3 σ for the region near C64-C80 disulfide bridge of three lysozyme structures determined from the data obtained with 19ID line focus beam at three different doses.

Stern, Joachimiak *et al.*, 19ID, 2012

Comparison of Monte Carlo simulations and our data

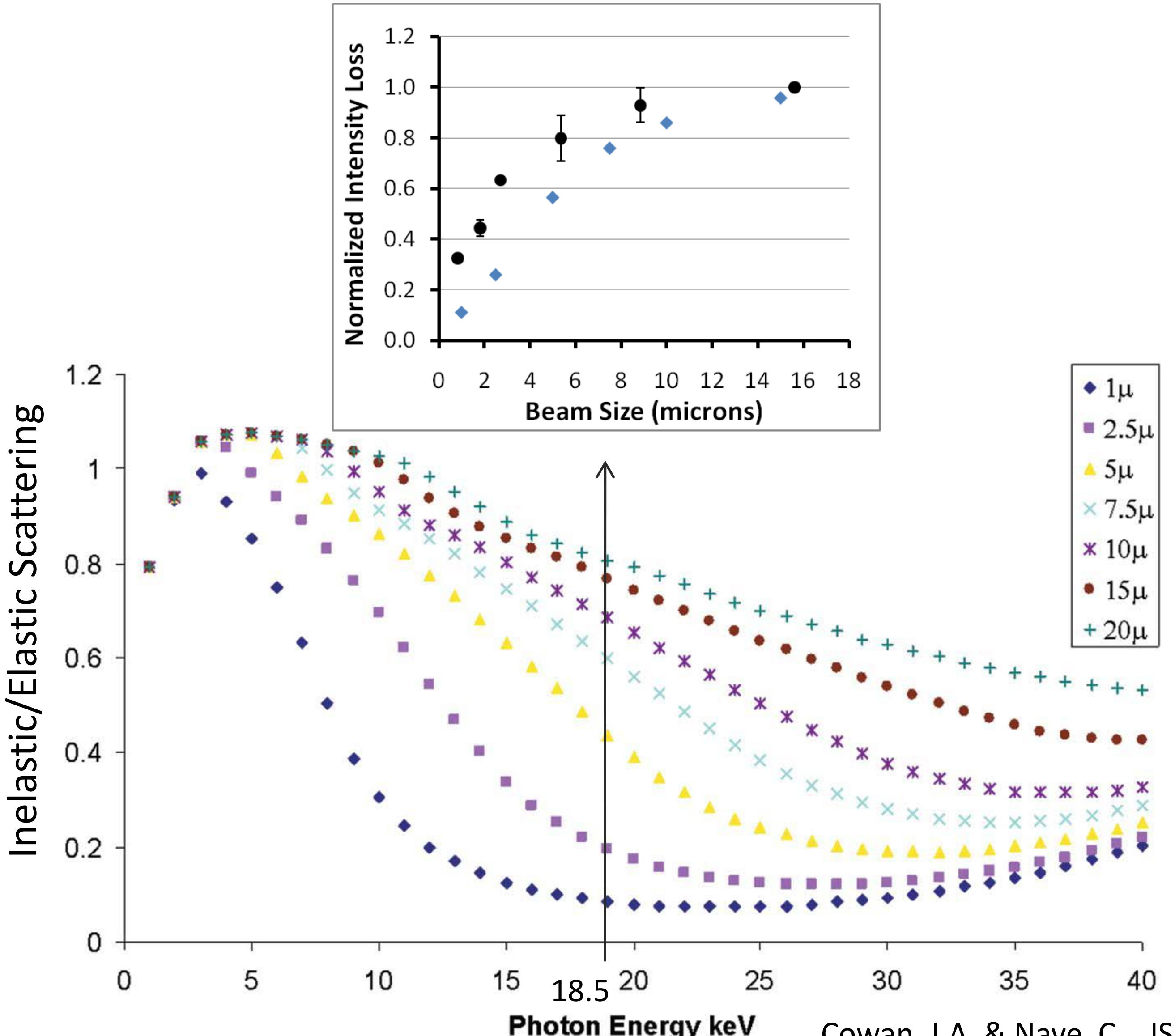

Cowan, J.A. & Nave, C., JSR **15**, 458-62 (2008).

APS-Upgrade

Benefits of the APS Upgrade

Increased beam current

- Pro - Increase intensity in to focus
- Con - Additional heat load on DCM

Improved beam stability

- Pro - Better spatial and/or temporal stability
- Con - N/A

New revolver undulator

- Pro – better match spectrum to experiment
- Con - $$

APS-Upgrade – higher current

23-ID-D
3.0 cm

12.0 keV 1st

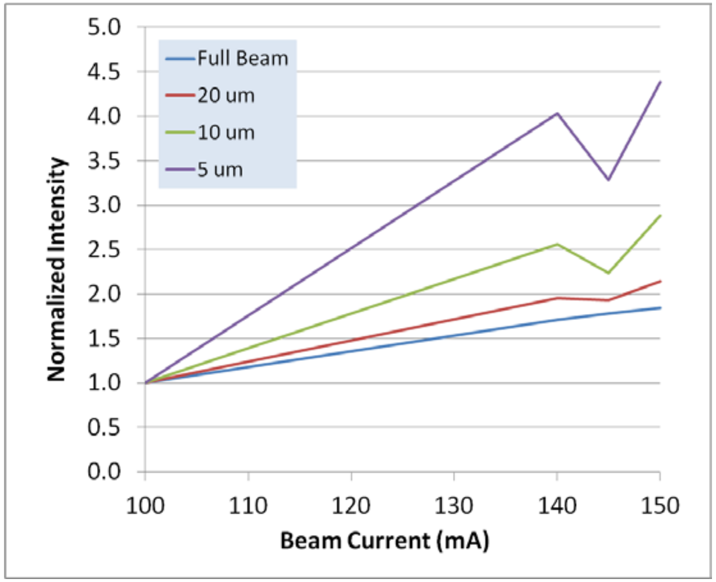

15.3 keV 3rd

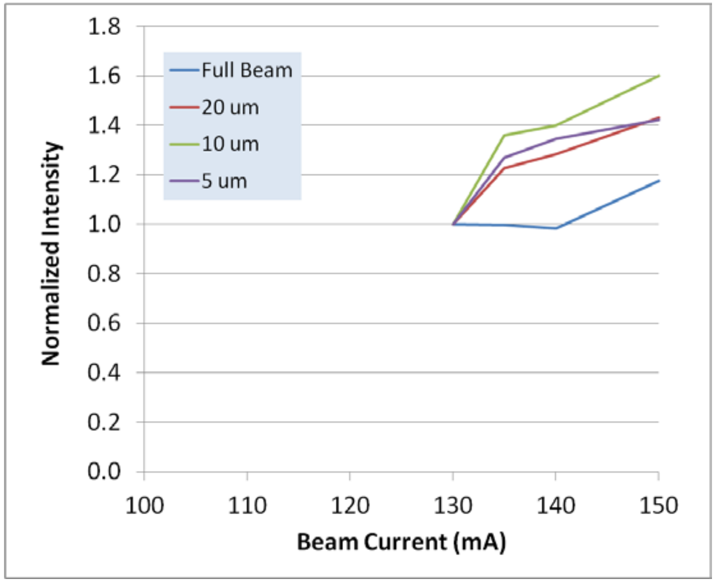

23-ID-B
3.3 cm

12.0 keV 1st

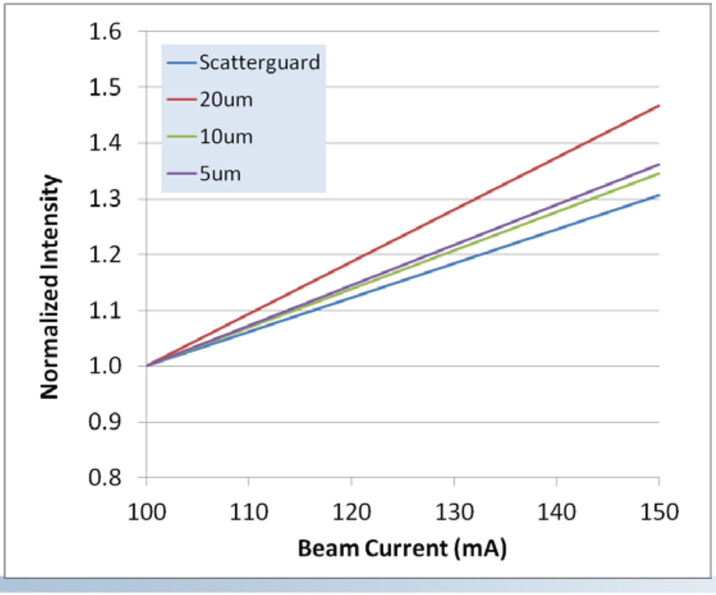

10.5 keV 3rd

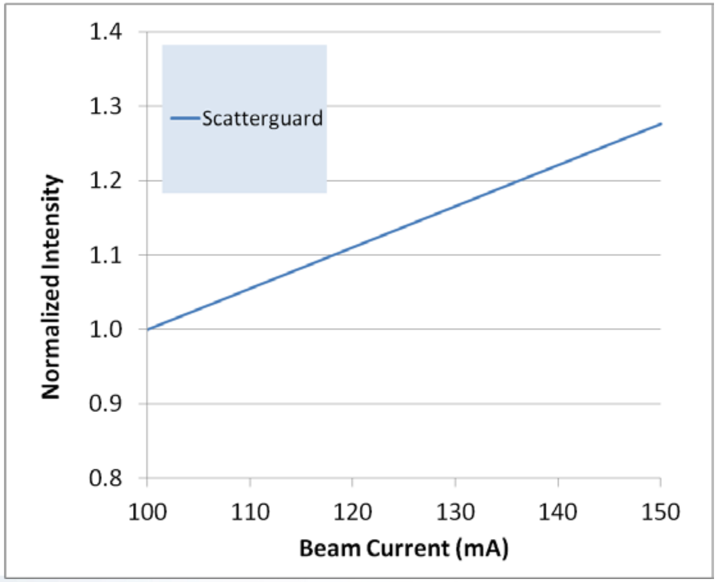

APS-Upgrade – higher current (continued)

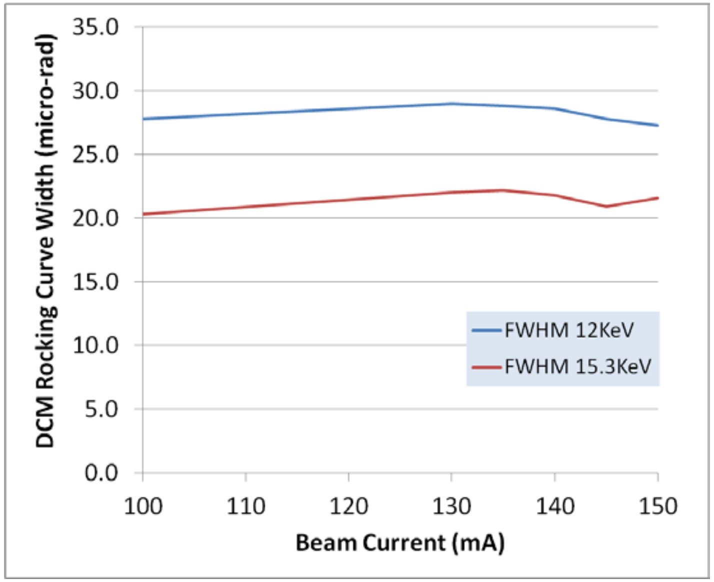

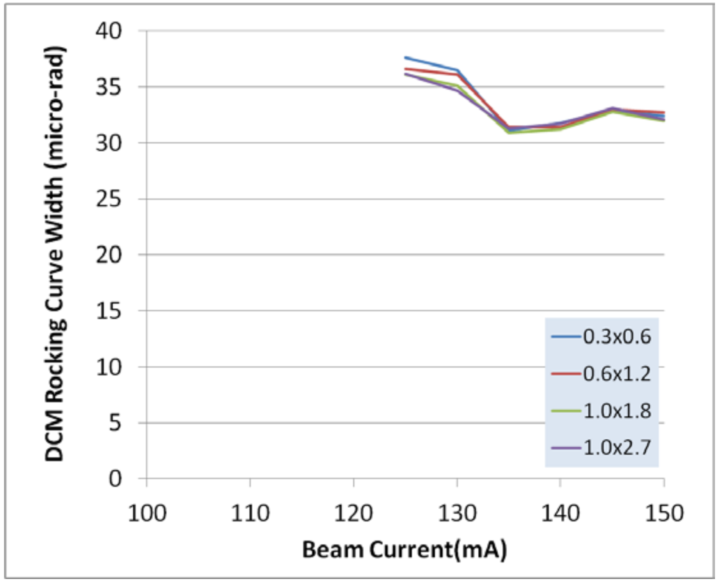

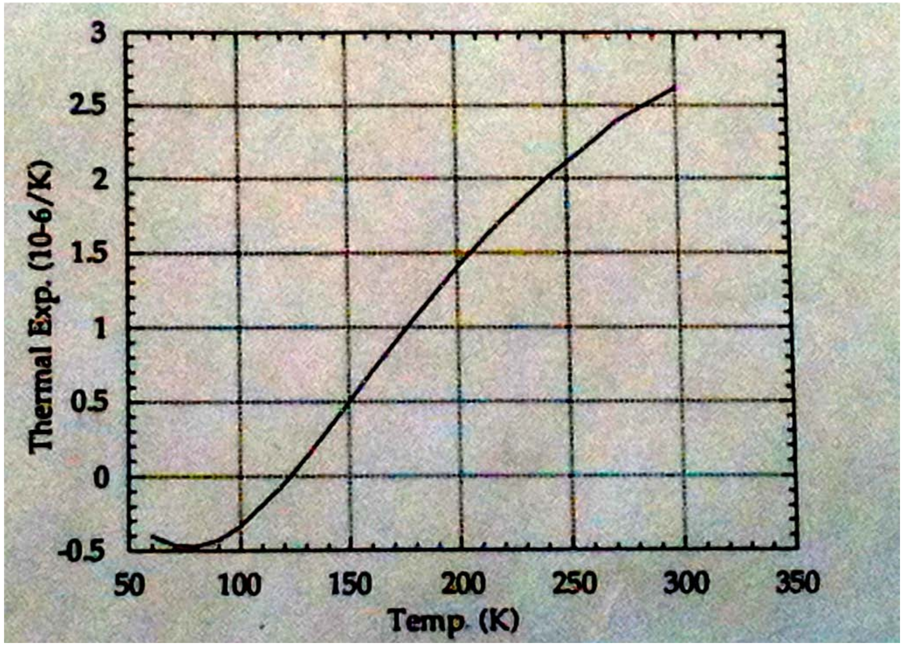

Operating micro-crystallography beamlines

Facility & beamline	Target beam size	Energy range	Approach
APS 23ID-B	5, 10, 20 μm	3.5-20 keV	Aperture
APS 23ID-D	5, 10, 20 μm	5-20 keV	Aperture
APS 17ID-B	10, 20 μm	6-20 keV	Aperture
APS 19ID	5, 10, 20 μm	6-17 keV	Aperture
APS 24ID-E	5-20 μm	12.66 keV	Aperture
APS 31ID	20 μm	9-13.8 keV	Aperture
Australia MX2	10 μm	5.5-28 keV	Aperture
CHESS A1	<20 μm	12.68 keV	Direct focus
CHESS F1	<20 μm	13.50 kev	Direct focus
CHESS F2	<20 μm	7-16 keV	Direct focus
Diamond I02	20 μm	5-25 keV	Aperture
Diamond I03	20 μm	5-25 keV	Aperture
Diamond I04	2x8 μm^2	13.1, 7.15 keV	Aperture
Diamond I24	7-10 μm	6.5-18 keV	Secondary source
ESRF ID13 EHII	1 μm	5-17 keV	Direct focus
ESRF ID23-2	10 μm	14.2 keV	Direct focus
ESRF ID29	10, 20 μm	6-20 keV	Aperture
Photon Factory BL-17A	20 μm	5.9-13.8 keV	Aperture
Photon Factory BL-1A	10 μm	2.7-3.0 keV	Aperture
SPring-8 BL32XU	1-10 μm	8.5-20 keV	Divergence-limited source
SPring-8 BL41XU	10 μm	6.5-35 keV	Aperture
SLS X06SA	(15)x5 μm^2	5.7-17.5 keV	(Aperture) direct focus
SSRL 12-2	7, 10, 20 μm	6.7-17.2 keV	Aperture

All dimensions are FWHM. (HxV) Selectable beam sizes are designated by comma-separated discrete sizes or by a size range.
Beamlines with beams of dimension 20 μm or smaller; some also produce larger beams.

Micro-crystallography beamlines – under development

Beamlines in process			Status
ALBA BL13	300x7 μm^2	5-21 keV	Commissioning
Diamond I02	20, 10 μm	7-17 keV	Commissioning
Diamond I03	20, 10 μm	7-17 keV	Commissioning
Diamond I04	20, 10 μm	7-17 keV	Commissioning
PETRA III MX1	5, 10 μm; 28x13 μm^2	5-17 keV	Commissioning
PETRA III MX2	4x1 μm^2	7-35 keV	Commissioning
APS 23ID-D	1-20 μm	6-35 keV	Construction
NSRRC PX	1-50 μm	5.7-20 keV	Construction
SOLEIL PX2	20 μm^2	5-15 keV	Construction
SSRF NFPS	10x5 μm^2	5-18 keV	Construction
MAX IV BioMAX	20 μm	5-25 keV	Design
NSLS II FMX	1-100 μm	5-20 keV	Design
NSLS II AMX	5-300 μm	5-25 keV	Design
NSLS II NYX	5-50 μm	3.5-17.5 keV	Design

GM/CA@APS Staff

www.gmca.aps.anl.gov

From left to right:
Mark Hilgart
Craig Ogata
Robert Fischetti
Sergey Stepanov
Dale Ferguson
Janet Smith
Oleg Makarov
Shenglan Xu
Michael Becker and
Sudhir Babu Pothineni

Insets left to right:
Sheila Trznadel
Ruslan (Nukri) Sanishvili
Naga Venugopalan and
Stephen Corcoran

Thank you for your attention

Thank you for your attention

www.gmca.aps.anl.gov